JOURNAL OF GEOPHYSICAL RESEARCH, VOL. 99, NO. D1, PAGES 1187–1210, JANUARY 20, 1994

Evaluation of water vapor distribution in general circulation models using satellite observations

Brian J. Soden[1]

Department of the Geophysical Sciences, University of Chicago, Chicago, Illinois

Francis P. Bretherton

Space Science and Engineering Center, University of Wisconsin, Madison

This paper presents a comparison of the water vapor distribution obtained from two general circulation models, the European Centre for Medium-Range Weather Forecasts (ECMWF) model and the National Center for Atmospheric Reseach (NCAR) Community Climate Model (CCM), with satellite observations of total precipitable water (TPW) from SSM/I and upper tropospheric relative humidity (UTH) from GOES. Overall, both models are successful in capturing the primary features of the observed water vapor distribution and its seasonal variation. For the ECMWF model, however, a systematic moist bias in TPW is noted over well-known stratocumulus regions in the eastern subtropical oceans. Comparison with radiosonde profiles suggests that this problem is attributable to difficulties in modeling the shallowness of the boundary layer and large vertical water vapor gradients which characterize these regions. In comparison, the CCM is more successful in capturing the low values of TPW in the stratocumulus regions, although it tends to exhibit a dry bias over the eastern half of the subtropical oceans and a corresponding moist bias in the western half. The CCM also significantly overestimates the daily variability of the moisture fields in convective regions, suggesting a problem in simulating the temporal nature of moisture transport by deep convection. Comparison of the monthly mean UTH distribution indicates generally larger discrepancies than were noted for TPW owing to the greater influence of large-scale dynamical processes in determining the distribution of UTH. In particular, the ECMWF model exhibits a distinct dry bias along the ITCZ and a moist bias over the subtropical descending branches of the Hadley cell, suggesting an underprediction in the strength of the Hadley circulation. The CCM, on the other hand, demonstrates greater discrepancies in UTH than are observed for the ECMWF model, but none that are as clearly correlated with well-known features of the large-scale circulation.

1. Introduction

Water vapor is the most variable constituent of the atmosphere, yet it plays a pivotal role in many aspects of the Earth's climate. Water vapor is the principal greenhouse gas, absorbing radiation throughout a broad portion of the IR spectrum. The increase in absorption by water vapor with increasing sea surface temperature, commonly referred to as water vapor feedback, greatly influences the sensitivity of the Earth's climate and is estimated to amplify the global warming due to a doubling of CO_2 by a factor of 1.6 [*Intergovernmental Panel on Climate Change*, 1990]. Aside from its direct radiative impact, water vapor also affects the climate system through its connection with other components of the hydrologic cycle. The vertical distribution of water vapor and its horizontal convergence are essential ingredients in predicting atmospheric stability and the occurrence of cumulus convection. Evaporation of water from the surface accounts for roughly 50% of the total surface cooling, while the subsequent release of latent heat during condensation contributes roughly one third of the total atmospheric thermal energy [*Chahine*, 1992]. The clouds formed as a result of the condensation processes also modify the radiative energy balance in a competing fashion. In the IR spectrum, clouds warm the planet by absorbing upwelling terrestrial radiation and emitting to space at the colder cloud top temperature, whereas in the visible spectrum, clouds cool the planet by reflecting incident solar radiation back to space. This link between water vapor and clouds, particularly at the larger spatial scales typical of general circulation models (GCMs), is a topic of considerable interest owing to the present uncertainty surrounding the role of cloud feedback in determining climate sensitivity [*Cess et al.*, 1990].

The importance of water vapor as a climate variable and its relation to other hydrologic processes, coupled with the necessitated reliance upon GCMs as climate prediction tools, underscores the need for GCMs to be able to accurately predict the distribution of water vapor and its spatial and temporal variations. However, despite this importance, there so far have been only a handful of evaluations of GCM water vapor climatologies [*Gaffen and Barnett*, 1992; *Liu et al.*, 1992]. One reason for

[1] Now with the Atmospheric and Oceanic Sciences Program, Princeton University, Princeton, New Jersey.

Paper number 93JD02912.
0148-0227/93/94JD-02912$05.00

the lack of comparisons is that water vapor is poorly measured on a global scale, particularly over oceans, where radiosonde data are scarce, and in the upper troposphere, where conventional radiosonde sensors are unreliable [*Elliot and Gaffen*, 1991]. Fortunately, in recent years extensive satellite archives which provide both a reliable source of water vapor data and near-global coverage have become available.

The ability to accurately measure the column integrated mass of water vapor (or total precipitable water (TPW)) from passive microwave sensors is well documented [*Staelin et al.*, 1976; *Grody et al.*, 1980; *Prabhakara et al.*, 1982; *Alishouse et al.*, 1990]. However, since the saturation vapor pressure of water decreases exponentially with decreasing temperature, the vertically integrated mass of water vapor largely reflects the amount of water vapor in the lower troposphere. Moreover, recent studies [*Lindzen*, 1990; *Rind et al.*, 1991; *Kiehl and Briegleb*, 1992] have emphasized the importance of upper tropospheric water vapor in regulating the trapping of IR radiation by the atmosphere. Therefore it is essential that any validation of the GCM-simulated water vapor distribution not only examine the TPW but also evaluate the ability of the model to represent the distribution of upper tropospheric water vapor. This is particularly important since TPW is closely tied to the local sea surface temperature [*Raval and Ramanathan*, 1989; *Stephens*, 1990], which is often prescribed in GCMs, whereas upper tropospheric water vapor is strongly influenced by the large-scale atmospheric circulation. Fortunately, measurements of upper tropospheric water vapor are routinely by provided satellite observations of spectral radiances in the 6.3-μm water vapor absorption band. Recent investigations have described summary data sets of clear-sky water vapor radiances obtained from geostationary (GOES [*Soden and Bretherton*, 1993] and Meteosat [*Schmetz and Turpeinen*, 1988]) and polar orbiting (NOAA [*Wu et al.*, 1992]) satellite platforms. These data sets provide a valuable source of upper tropospheric water vapor observations which are suitable for comparison with forward calculated radiances determined from GCM profiles of temperature and moisture.

The objective of this study is to evaluate the ability of two GCMs to simulate the distribution of both TPW and upper tropospheric water vapor, using satellite observations of TPW from the Special Sensor Microwave / Imager (SSM/I) and 6.7-μm brightness temperature ($T_{6.7}$) from GOES. The time periods examined in this study are July 9 - August 8, 1987, and January 12 - February 11, 1988. For brevity, these two periods are hereafter referred to as July 1987 and January 1988, respectively. The model results examined in this study consist of daily uninitialized analyses obtained from the European Centre for Medium-Range Weather Forecasts (ECMWF) model and GCM simulations performed by the National Center for Atmospheric Research Community Climate Model version 2 (NCAR CCM). Although both the ECMWF model and the CCM are collectively referred to as GCMs, the results examined are of fundamentally different character in that the ECMWF analyses are constrained by daily observations of temperature, wind and moisture, whereas the CCM simulations are not. Hence this comparison is not intended to indicate which GCM is better but rather to demonstrate a methodology for using satellite observations to evaluate the water vapor distribution in GCMs. Specifically, we compare both the geographic distribution and the temporal variation of TPW and $T_{6.7}$ simulated by the GCMs with the respective satellite-measured quantities. Section 2 describes the satellite data sources used in this investigation and relevant aspects of the GCMs are discussed in section 3. The monthly mean and temporal variabilities of TPW and $T_{6.7}$ are compared in sections 4 and 5, respectively. Section 6 examines the ability of the ECMWF model to simulate the observed synoptic progression of TPW and upper tropospheric water vapor.

2. Satellite Observations

2.1. SSM/I Total Precipitable Water

The SSM/I is a passive remote sensing microwave radiometer which measures upwelling radiation in four spectral channels: 19, 22, 37, and 85 GHz. The retrieval of total precipitable water by the SSM/I is made possible by the presence of a water vapor absorption band centered at 22.235 GHz. At this frequency the emissivity of the ocean surface is quite low (approximately 0.5). As a result the oceans provide a radiatively cold background against which the increased emission from water vapor can be compared. The microwave emission at this frequency increases with increasing precipitable water, providing a sharp contrast with the much lower and highly polarized emission from the ocean surface. The upwelling radiation in the 19- and 37-GHz channels, however, is significantly less sensitive to the amount of water vapor. As a result, the brightness temperature difference between the 22- and 19- or 37-GHz channels provides a measure of the amount of absorption due to atmospheric water vapor. This principle is exploited by combining measurements centered on 22.235-GHz water vapor absorption band with those at adjacent frequencies containing markedly different water vapor emission dependencies to retrieve total precipitable water. This study uses the National Environmental Satellite Data and Information Service (NESDIS) algorithm [*Alishouse et al.*, 1990] to derive TPW from SSM/I brightness temperature measurements. Microwave observations of TPW are generally considered to provide the best global measurements available. Uncertainties in the retrieved TPW are typically on the order of 2-3 kg/m^2 [*Alishouse et al.*, 1990; *Prabhakara et al.*, 1982]. Because of large variations in surface emissivity, TPW is not retrieved over land or over ice covered oceans. A distinct advantage of microwave TPW retrievals is that the upwelling radiation is insensitive to scattering by cloud droplets; hence TPW can be accurately measured under cloudy conditions. However, for larger precipitation-size particles, scattering effects are no longer negligible and conditions of heavy precipitation must be excluded from the retrieval. In this study the criteria for identifying conditions of heavy precipitation follow those of *Hollinger et al.* [1987]. Typically these criteria result in the exclusion of less than 10% of the available observations. Further details on the SSM/I instrumentation and estimation of TPW are given by *Hollinger et al.* [1987] and *Alishouse et al.* [1990].

2.2. GOES 6.7-μm Brightness Temperature

This study utilizes observations in the 6.7-μm spectral channel obtained from the GOES-east satellite for the

periods July 1987 and January 1988. The 6.7-μm channel is located near the center of a strong water vapor absorption band and under clear-sky conditions is sensitive primarily to the relative humidity averaged over a depth of atmosphere extending from roughly 200-500 mbar. Figure 1 illustrates the approximate sensitivity of the 6.7-μm brightness temperature $T_{6.7}$ to changes in relative humidity at various pressures for a typical tropical profile viewed at zenith. To determine the clear-sky radiance at 6.7 μm, the local spatial structure of the radiance field at 11 μm and the observed correlation between the 11-μm and 6.7-μm radiances are used to discriminate between clear and cloudy pixels. This approach has been demonstrated to be more reliable than cloud clearance based solely upon the local spatial structure of the clear-sky 6.7-μm channel alone and to provide estimates of the clear-sky $T_{6.7}$ which are repeatable from successive images 30 minutes apart to within roughly 1 K [*Soden and Bretherton*, 1993]. The random error introduced by the cloud clearance algorithm is therefore estimated to be at or below this level. Details regarding the GOES 6.7-μm channel and cloud clearance procedure are provided by *Soden and Bretherton* [1993].

An unfortunate consequence of any cloud clearance procedure is the potential to introduce into the data a sampling bias due to a lack of observations from overcast pixels. The magnitude of such a bias is extremely difficult to determine from the observed data; however, a rough estimate of this sampling bias can be obtained by simulating a similar bias using ECMWF data. For this purpose, the monthly mean 6.7-μm brightness temperature calculated from ECMWF profiles of temperature and humidity are averaged over all grid boxes and compared with those values averaged only from grid boxes in which there was also a corresponding clear-sky estimate available from the GOES 6.7-μm channel for that day and time. The differences in monthly mean $T_{6.7}$ for July 1987 are zonally averaged for selected latitude belts and shown in Table 1. As expected, the biases are negative, suggesting that the procedure of cloud clearing introduces a slight warm (dry) sampling bias ranging from -0.52 K for the southern hemisphere midlatitudes to near zero in the winter subtropics. It is noted, however, that these values represent only a very crude estimate of the actual sampling bias and therefore should be interpreted with some caution.

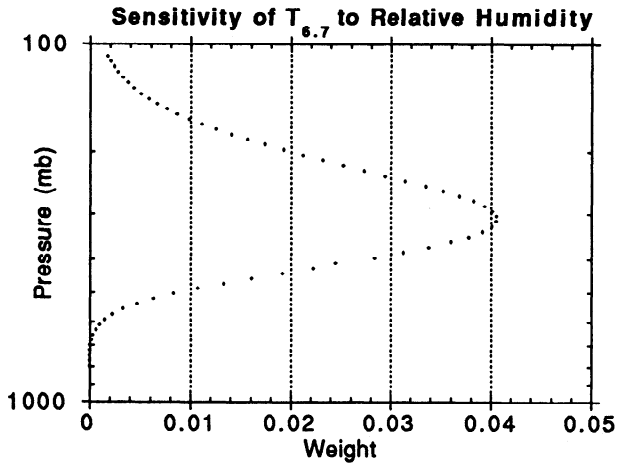

Fig. 1. Sensitivity of $T_{6.7}$ to local variations in relative humidity. The sum of weights for individual points is unity.

Although clear-sky $T_{6.7}$ is strongly correlated to the upper tropospheric relative humidity, the most reliable procedure for validating the distribution of upper tropospheric water vapor simulated by a GCM is to compare the observed clear-sky $T_{6.7}$ with that calculated by a radiative transfer model using the GCM profiles of temperature and moisture as input. In this study, the latest University of Wisconsin-Cooperative Institute for Meteorological Satellite Studies (CIMSS) transmittance model is used to perform the forward calculations. The CIMSS research model is a 40-level, multivariate regression model based upon FASCOD3 line-by-line transmittance calculations and is functionally similar to that described by *Eyre* [1991]. To perform the calculations, the profiles of temperature and moisture are interpolated from the GCM levels onto the 40 levels required for the transmittance model. Comparison of the forward calculations with FASCOD3 line-by-line computations suggests random errors in the calculated brightness temperatures of approximately 1-1.5 K (H. Woolf, CIMSS, personal communication, 1993).

3. MODELS

3.1. ECMWF Model

This study utilizes global, uninitialized analyses obtained from the ECMWF basic level III archive. The ECMWF forecast model is a 19-level spectral model with horizontal resolution truncated at wavenumber 106. Surface boundary conditions are prescribed from analyzed sea surface temperatures and snow cover, while land surface temperatures are predicted internally. The analysis system is a three-dimensional optimal interpolation scheme which combines model forecasts based on 6-hour prior analyses with current observations from surface, radiosonde, and satellite-based platforms. In the absence of observational data, the forecast is treated as the most likely state of the atmosphere. Imbalances between winds and temperature-pressure fields associated with observational noise or inadequate sampling are aliased into gravity waves which are subsequently dispersed by the model. The corresponding vertical displacements which directly affect the relative humidity are presumably approximately randomly distributed with a near-zero mean, becoming indistinguishable from a high frequency background. The satellite data consist of profiles of temperature and precipitable water obtained from the TIROS Operational Vertical Sounder (TOVS). During the periods examined in this study, TOVS water vapor profiles, when available, were given roughly equal weight with model forecasts. However, in January 1989, the weighting attached to TOVS moisture retrievals was reduced because of their negative impact on model forecasts in the northern hemisphere [*Zhang et al.*, 1989]. The analyses are assimilated twice per day at 0000 and 1200 UT and transformed onto a reduced resolution (2.5° by 2.5°) rectangular grid. Vertically, the fields are interpolated from the model σ levels to 14 standard pressure levels (1000, 850, 700, 500, 400, 300, 250, 200, 150, 100, 50, 30, 20, and 10 mbar).

The assimilation procedure employed at ECMWF has undergone numerous changes over time [see *Trenberth and Olson*, 1988]. Of particular relevance to this study are the changes in the physical parameterizations of clouds, convection and condensation in May 1985 and the inclusion of TOVS precipitable water profiles into the analysis

system in March of 1986. The changes in physical parameterizations greatly enhanced the vertical motions in convective regions, resulting in a 50% increase in the strength of the Hadley circulation, a reduction of moisture in the boundary layer and above 850 mbar, and an increase in moisture at 850 mbar [*Trenberth and Olson*, 1988; *Brankovic*, 1986]. *Illari* [1989] concluded that the inclusion of TOVS precipitable water profiles moistened the analysis over ocean regions. In a later study, *Zhang et al.* [1989] obtained the opposite conclusion, indicating that the model first guess was too moist and attributed the discrepancy with *Illari* [1989] to a change in the humidity analysis scheme from a two-dimensional correction scheme to the three-dimensional optimal interpolation scheme in September 1986. This result further highlights the transient and assimilation dependent nature of the moisture analyses and suggests that the results of this comparison may be applicable only for the period May 1986 to May 1989, during which time the assimilation procedure remained fairly stable, closely resembling that used in the present study.

3.2. NCAR CCM

This study also examines simulations from the NCAR CCM version 2. This is the most recent version of the CCM and, with respect to previous versions, represents a considerably different GCM in terms of both the parameterized physics and the resolved dynamics. The CCM is an 18-level spectral model run at a horizontal resolution of T42, which is roughly equivalent to a 2.8^o by 2.8^o latitude-longitude grid. The simulations examined in this study are taken from a 10-year model run in which observed sea surface temperatures (SSTs) spanning the period from January 1979 to December 1988 were prescribed in the model. A complete description of the CCM version 2 and its changes relative to previous versions is provided by *Hack et al.* [1993]. Significant improvements in the radiation scheme, including a delta-Eddington model for radiative transfer and revised cloud parameterizations, have been included. However, the changes which are likely to have greatest impact on the water vapor distribution and hence are of the most interest for this study, include (1) the employment of a stability dependent mass-flux parameterization of cumulus convection which replaces the moist adiabatic adjustment procedure previously used, (2) the incorporation of an explicit, non-local boundary layer scheme in which the boundary layer height for each grid is diagnosed as a function of the bulk Richardson number and surface heat flux [*Holtslag and Boville*, 1993], and (3) the inclusion of a new water vapor advection scheme based upon semi-Lagrangian methods [*Rasch and Williamson*, 1990] which ameliorates some of the computational problems associated with spectral transport formulations.

It must be emphasized, however, that the ECMWF analyses and CCM simulations are of fundamentally different natures, since the ECMWF analyses benefit by the assimilation of daily temperature, moisture, and wind observations, whereas the CCM is constrained only by the seasonally appropriate boundary conditions. Therefore differences between the ECMWF analyses and CCM simulations may be attributed both to impact of the ECMWF assimilation procedure and to differences between the two GCMs. Hence this investigation is not intended to determine which model is best but rather to evaluate the predicted moisture fields independently while permitting some insight to be gained by associating differences between the moisture distributions with differences between certain aspects of the models (e.g., physical parameterizations, spatial resolution).

4. EVALUATION OF TOTAL PRECIPITABLE WATER

To assess the ability of the ECMWF analyses and CCM simulations to capture the distribution of lower tropospheric water vapor, we compare the spatial and temporal distributions of TPW with those observed by the SSM/I. In this section, monthly statistics of TPW for July 1987 and January 1988 are examined.

Since the CCM simulations are forced only with the observed SSTs and are not constrained by daily observations of pressure and wind as the ECMWF analyses are, it is useful to obtain some measure of the interannual variability of TPW in order to evaluate the significance of the differences between the CCM and SSM/I. The SSM/I observations are too short to evaluate the interannual variability, and changes in the ECMWF assimilation procedure may introduce spurious interannual variations. Therefore the standard deviation of monthly mean TPW from the CCM calculated from a 20-year model run subject to seasonal changes in external forcing and sea surface temperatures is utilized to estimate the interannual variability. Figure 2 shows the standard deviation of the monthly mean TPW for both July and January. For brevity the results have been zonally averaged. Typical interannual variations are of the order of 1-3 kg/m^2, with the higher values occurring primarily over the tropics and the lower values occuring toward the poles. This study will focus on those discrepancies which are greater than the model interannual variability.

4.1. Monthly Mean

The global distribution of monthly mean TPW from SSM/I observations, ECMWF analyses, and CCM simulations are shown for July 1987 (Figure 3*a*) and January 1988 (Figure 3*b*). Due to the uncertainty in TPW retrievals over

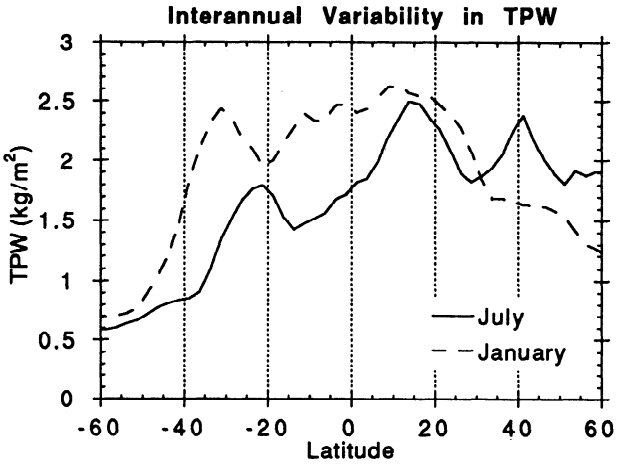

Fig. 2. The interannual standard deviation of monthly mean TPW determined from a 20-year CCM simulation. Units are kilograms per square meter.

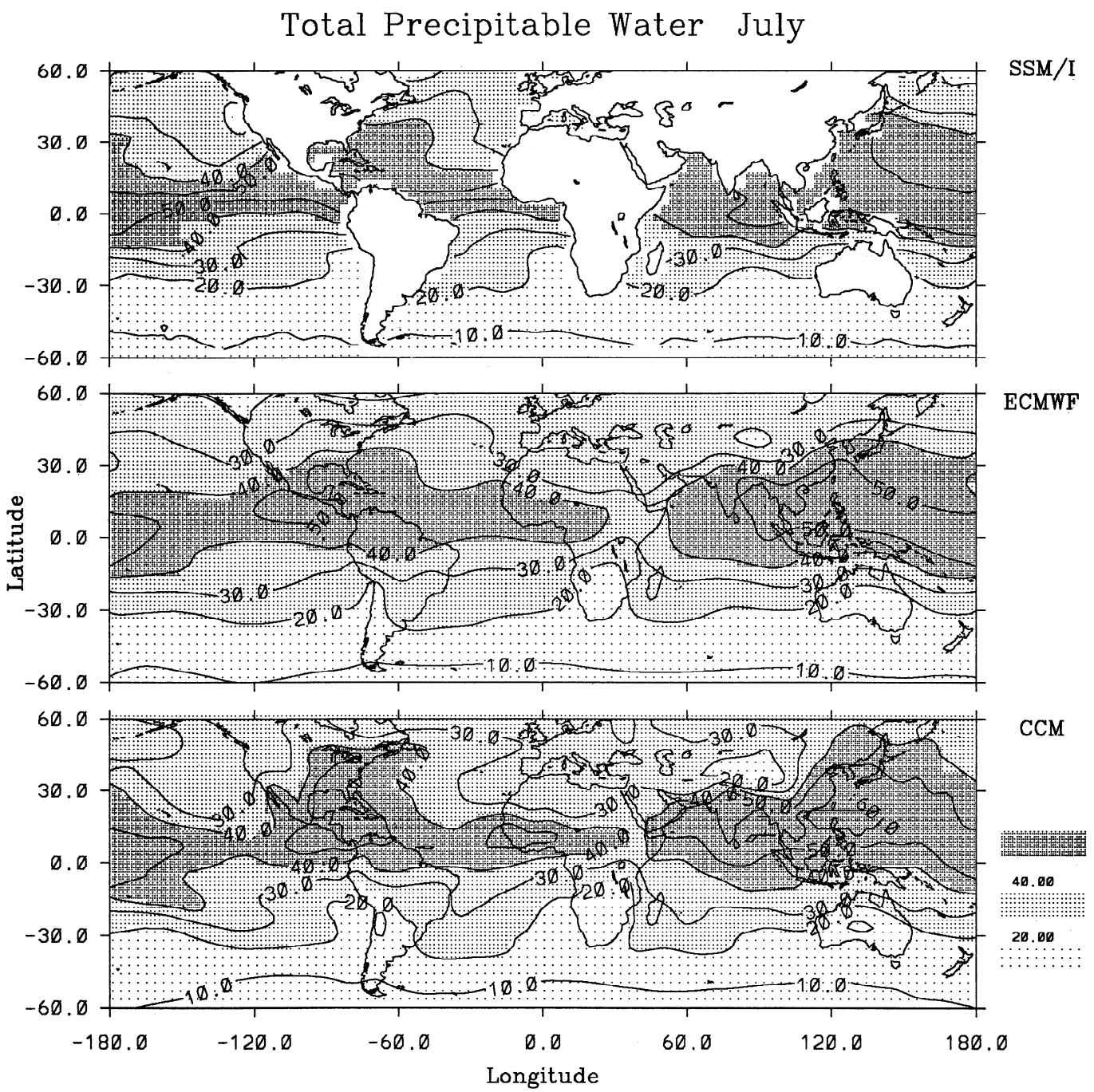

Fig. 3. The monthly mean TPW from SSM/I observations, ECMWF analyses, and CCM simulations for (a) July 1987 and (b) Janaury 1988. Units are kilograms per square meter.

ice, the comparison is restricted to latitudes equatorward of 60°. In both the July 1987 and the January 1988 periods, the SSM/I observations reveal a distinctly zonal pattern in the distribution of TPW. Maximum values in excess of 50 kg/m^2 occupy much of the tropics, highlighting the presence of the Intertropical Convergence Zone (ITCZ) and western Pacific warm pool, whereas minimum values ranging from 10-20 kg/m^2 dominate the mid- to high-latitude oceans, particularly in the winter hemisphere. These features emphasize the importance of warm SSTs and deep tropical convection in enhancing the TPW. Despite the strong latitudinal dependence in TPW there are obvious departures from zonal symmetry. Most notable are the moist bands which extend poleward from the tropics into the western midlatitude oceans and the adjacent dry tongues which coincide with the climatological positions of subtropical ridges off the west coasts of North and South Americas, Africa, and Europe. The moist bands highlight the transport of water vapor from the tropics to higher latitudes, whereas the dry tongues coincide with areas of cold oceanic upwelling. The cold SSTs combined with large-scale atmospheric subsidence acts to suppress atmospheric convection, producing a shallow marine boundary layer overlain by a very dry free atmosphere. The shallow-

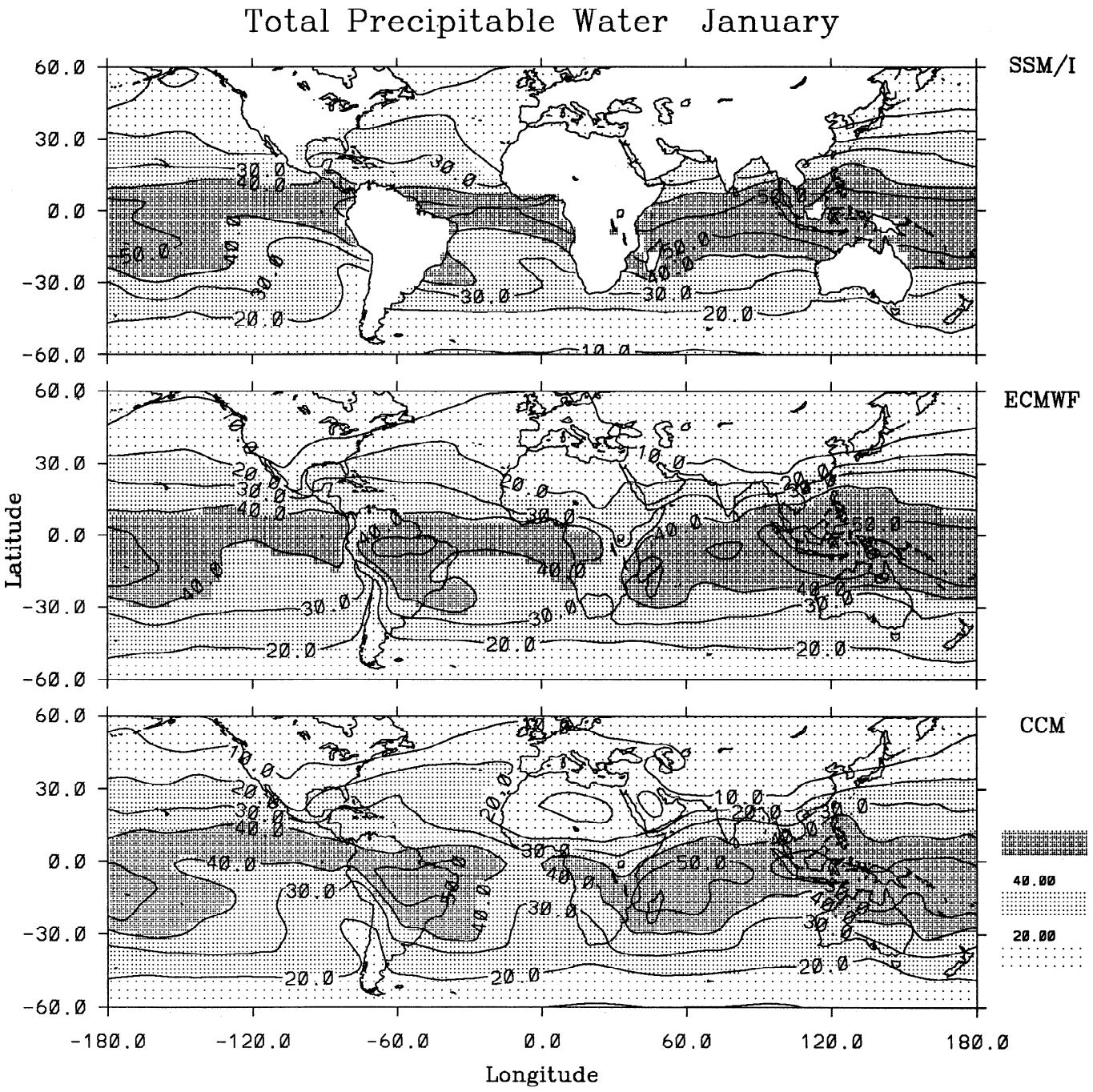

Fig. 3. (continued)

ness of the boundary layer and the dryness of the overlying free atmosphere both contribute to the low values of TPW for these regions.

The ECMWF analyses perform very well in capturing the primary features of monthly mean TPW and their seasonal variation. The ITCZ and western Pacific maxima agree well with observations, as do the positions and intensities of moist bands over extratropical oceans. Despite the overall agreement, however, some systematic discrepancies do exist. The most obvious problems are associated with the dry subtropical ridges off the west coasts of continents. In these areas the TPW in the analyses is frequently 1.5-2 times as large as that observed, contributing to a broadening of the ITCZ over the eastern Pacific and Atlantic oceans. This discrepancy was also noted recently by *Liu et al.* [1992]. Figure 4 compares the difference in monthly mean TPW between the observations and the analyses. A large moist bias is evident over all four previously discussed subtropical ridges in both seasons, indicating a systematic problem in predicting the dryness over the subtropical ridges. Given the relatively coarse vertical resolution of the model and the characteristic shallowness of the boundary layer in these regions, it is plausible that the discrepancies in TPW are attributable to difficulties in simulating the

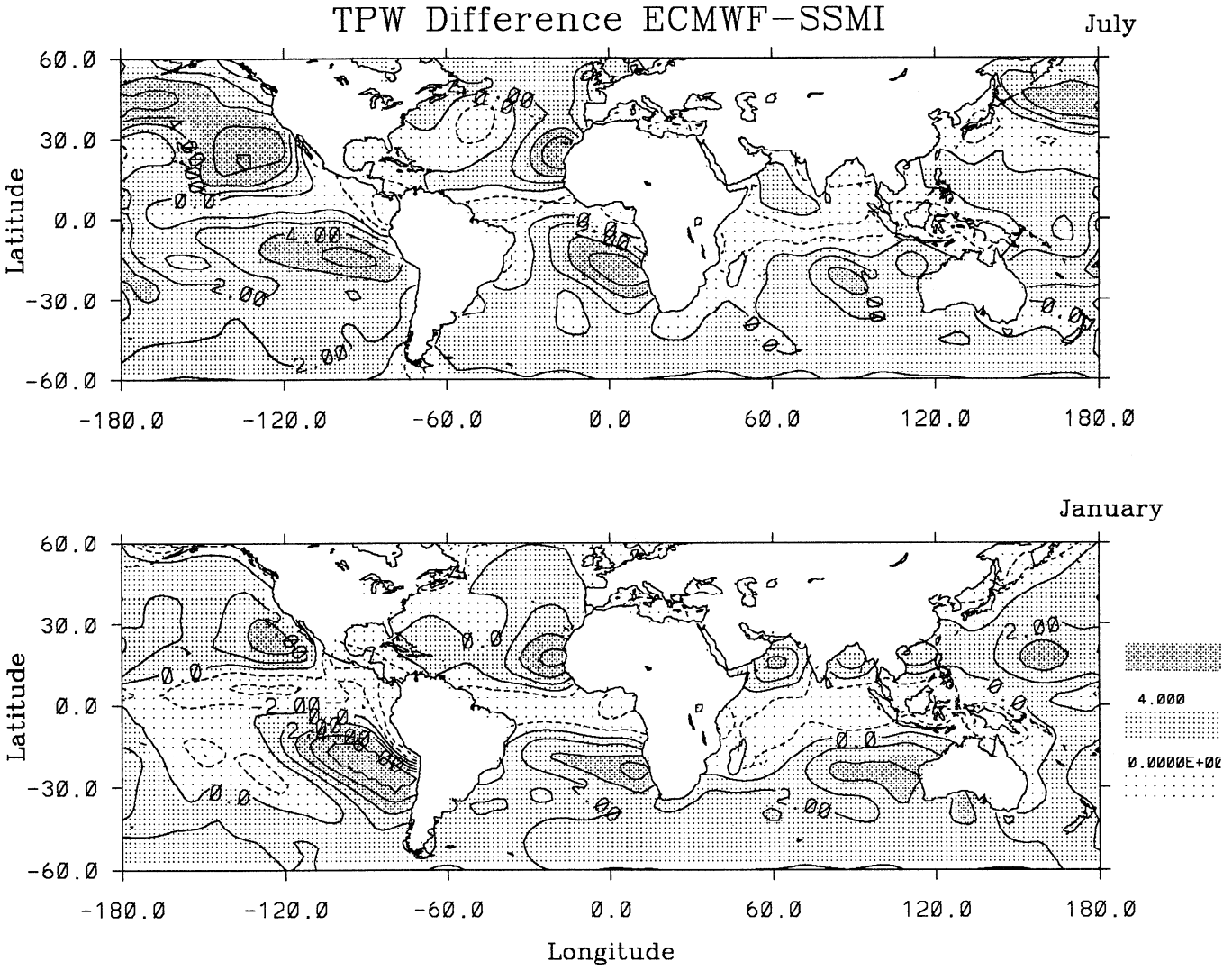

Fig. 4. Difference in TPW (ECMWF - SSM/I) for (top) July 1987 and (bottom) January 1988.

sharp vertical gradients in water vapor near the top of the boundary layer. To examine this possibility, monthly mean profiles of temperature, dew point, and water vapor mixing ratio taken from radiosonde (RAOB) ascents over the subtropical eastern Pacific are compared with the monthly mean profiles from the ECMWF in Figure 5. The RAOB shows a large gradient in specific humidity between 900 mbar and 950 mbar, with the mixing ratio reduced to 4.5 g/kg at 900 mbar. The ECMWF profile, on the other hand, contains no such gradient, simulating a monthly mean mixing ratio of 7.8 g/kg at 850 mbar, which is roughly twice that observed. Both the ECMWF and RAOB contain similar temperature profiles with a well-mixed boundary layer extending up to about 850 mbar, after which the temperature decreases approximately adiabatically. However, the RAOB dew point profile shows a much sharper decrease in the boundary layer than the ECMWF model does. Furthermore, the strength of the capping inversion is underestimated in the ECMWF model, encouraging a deeper boundary layer and hence larger TPW values. Although this represents only a single comparison, it does support the hypothesis that difficulty in representing the large gradients of moisture and temperature within the boundary layer are responsible for the discrepancies in the ECMWF TPW over the subtropical ridges.

It is also worth noting that the assimilation of TOVS retrievals into the analyses may actually contribute to the bias in TPW for these regions. Figure 6 shows the monthly mean difference between the SSM/I- and TOVS-retrieved TPW values. The TOVS data exhibit a bias similar to that observed for the ECMWF model, with distinctly larger values over the subtropical ridges. Differences between the SSM/I and TOVS TPW evident in Figure 6 may stem from errors in cloud clearance, which would tend to produce a colder brightness temperature and thus a moist bias in the retrieved TPW; from the use of a biased first guess in the retrieval owing to inadequate data for these regions; or from sampling differences, since the TOVS retrievals are available only from cloud-free regions.

Another important difference in Figure 4 is the systematic underprediction of TPW along the ITCZ during both July and January. A similar bias is evident in the TOVS data, suggesting a clear-sky sampling bias in the TOVS retrievals which may contribute to the lower TPW in the ECMWF model. Another cause of the model bias could be is a systematic underprediction in the amount of

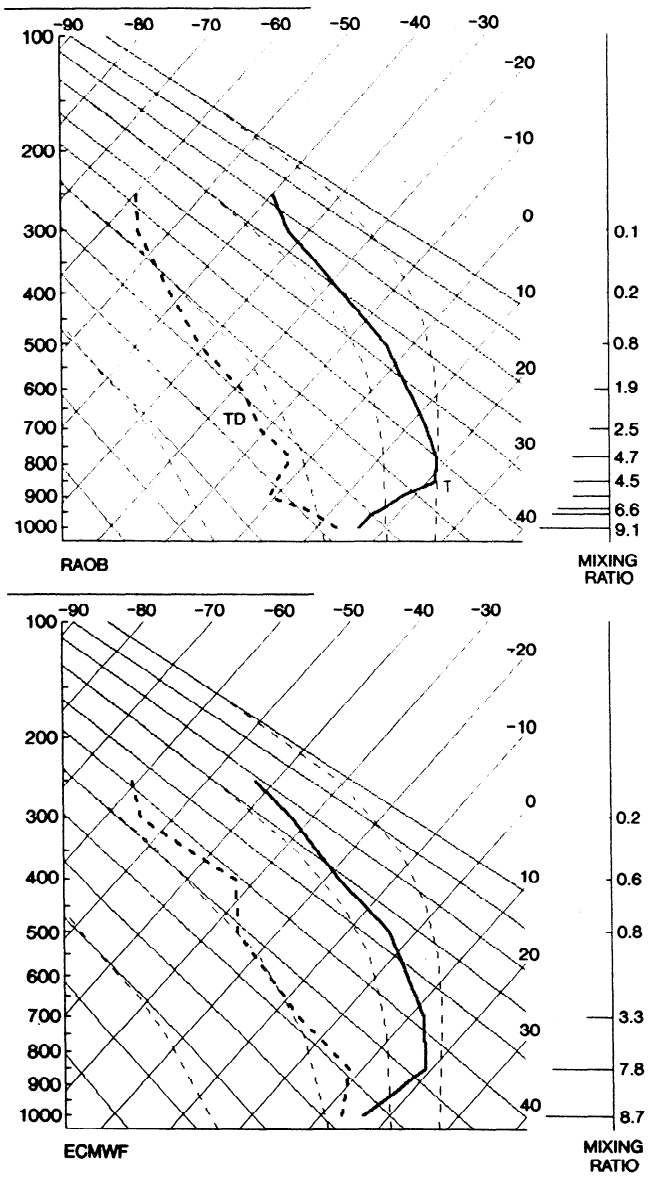

Fig. 5. Monthly mean profiles of temperature (solid line), dew point temperature (dashed line), and mixing ratio for 29° N, 119° W from (top) radiosonde observations and (bottom) ECMWF analyses.

water vapor transported by the model's Hadley circulation, resulting in decreased moisture convergence along the ITCZ and hence lower values of TPW. Further evidence supporting this hypothesis is presented in the upper tropospheric humidity comparison (section 4).

The CCM simulations also capture the chief features of the monthly mean TPW distributions and their seasonal variations. The ITCZ, western Pacific maxima, extratropical moist bands, and distinct latitudinal gradient in TPW are all clearly present in the modeled distribution. Interestingly, in comparison to the ECMWF model, the CCM does a noticeably better job of capturing the narrowing of the ITCZ and the dryness of the eastern subtropical Pacific and Atlantic oceans. The better agreement may be attributable to the inclusion of an explicit boundary layer parameterization in the CCM, which has been shown to have a significant impact upon the moisture profiles of the lower troposphere [*Holtslag and Boville*, 1993]. Despite this success, there are noticeable differences between the CCM and SSM/I TPW distributions. Over the summer hemisphere subtropics there is a tendency for the TPW to be overestimated in the western portion of the ocean basins and underestimated in the eastern portion of the basins. A clearer depiction of these discrepancies is given in Figure 7, which shows the difference between the CCM and SSM/I values (CCM - SSM/I). The east-west discrepancies in TPW found in the summer hemisphere subtropical ocean basins are nearly twice as large as the estimated interannual variability (Figure 2), suggesting that they represent a real bias in the model. Inspection of the CCM and ECMWF pressure fields (not shown) indicates that the CCM overestimates the pressure of the subtropical highs in these regions. The enhanced anticyclonic circulation generates stronger dry-air advection over the eastern half of the basins and stronger moist-air advection over the western half which is consistent with the observed pattern of discrepancy.

4.2. Thermodynamic Versus Dynamic Influences

The distinct zonal pattern of TPW evident in Figure 3 largely reflects the distribution of SST and highlights the strong thermodynamic regulation of TPW [*Prabhakara et al.*, 1979; *Stephens*, 1990]. This regulation stems from the dependence of the saturation mixing ratio on atmospheric temperature through the Clausius-Clapeyron relationship. Given the strong correlation between SST and TPW, the good agreement between the modeled and observed distributions of TPW demonstrated above is at least partially a reflection of the fact that observed SSTs were prescribed in both models. To examine the influence of atmospheric dynamics on the distribution of TPW, it is useful to discriminate between the TPW due to dynamical processes and that due to thermodynamic processes. Toward this end, *Prabhakara et al.* [1979] and *Stephens* [1990] have defined a normalized precipitable water parameter

$$\mathrm{TPW}^* = \frac{(\mathrm{TPW} - \mathrm{TPW}')}{\mathrm{TPW}} \tag{1}$$

which measures the relative contribution of dynamical influences to the observed TPW. Following *Stephens* [1990], the parameter TPW′ in (1) is the total precipitable water predicted using a simplified model based upon an approximate version of the Clausius-Clapeyron relationship:

$$\mathrm{TPW}' = 10.82\frac{r}{(1+\lambda)}e^{(0.064T_s - 288)} \tag{2}$$

where T_s is the SST, r is relative humidity and λ is the ratio of the atmospheric scale height to the scale height of water vapor and has a typical value of 3.5. The factor $r/(1+\lambda)$ is determined by performing a least squares regression between SSM/I observations of TPW and the right-hand side of (2) using National Meteorological Center SSTs and is assigned a value of 0.178 in this study.

Figures 8*a* and 8*b* illustrate the global distribution of monthly mean TPW* from SSM/I observations, ECMWF analyses, and CCM simulations for July 1987 and January 1988. The values are expressed in terms of a percentage

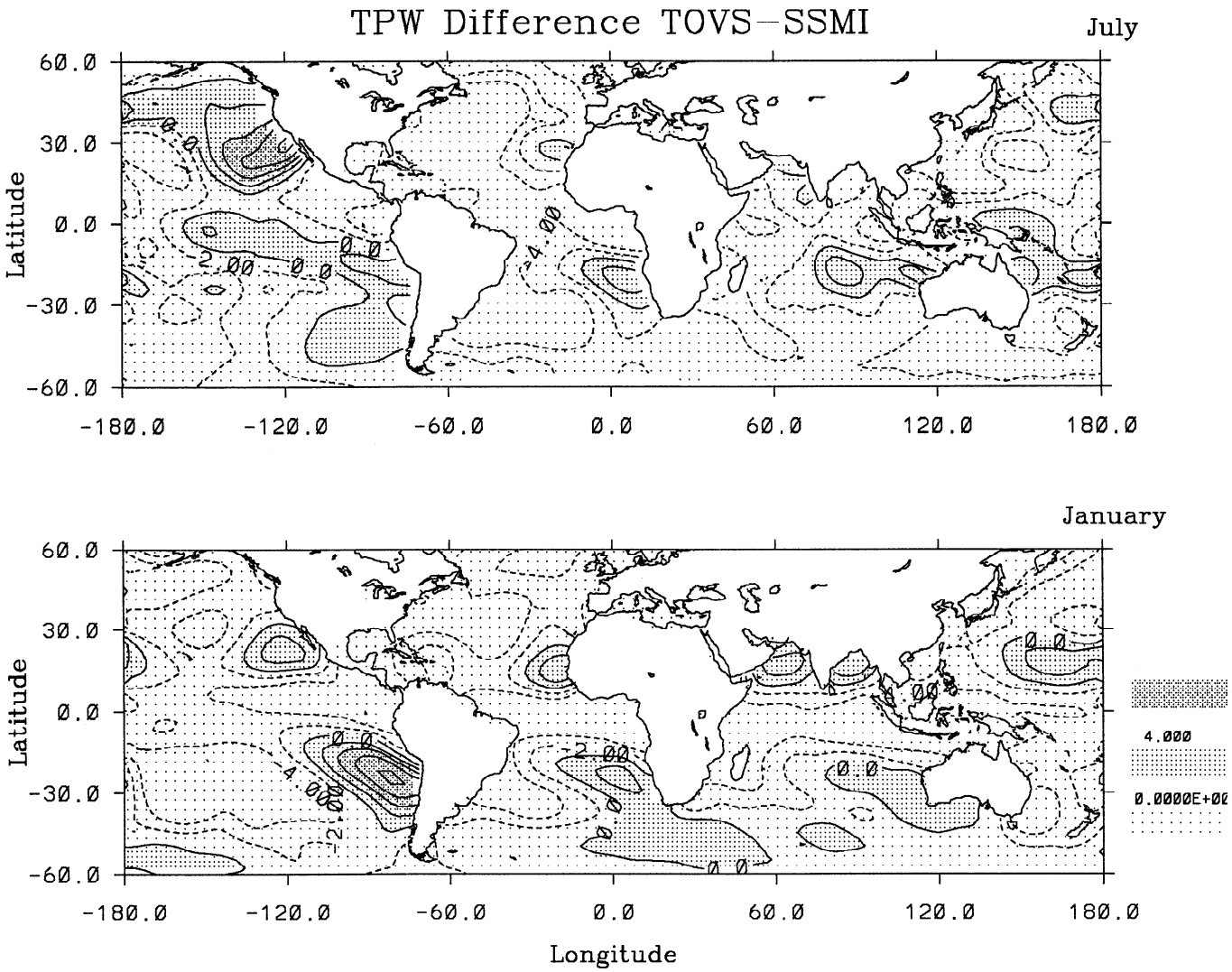

Fig. 6. Difference in TPW (TOVS - SSM/I) for (top) July 1987 and (bottom) January 1988.

ranging from -60% to 60%. Values of TPW* greater than zero indicate a greater than average relative humidity for that T_s or a relatively unstable lapse rate. Both the observations and the model simulations exhibit similar distributions of TPW* which highlight several features of the large-scale circulation. The primary features in both the models and observations are (1) a maximum in TPW* over the summer hemisphere midlatitudes, reflecting enhanced moisture transport by transient eddies associated with the midlatitude storms tracks; (2) markedly lower values of TPW* over the winter hemisphere midlatitudes, particularly in the northern hemisphere where dry air is advected from cold wintertime land masses over the warmer adjacent oceans [*Stephens, 1990*]; (3) smaller positive values of TPW* highlighting moisture convergence along the ITCZ; and (4) negative values of TPW* over the eastern subtropical oceans where large-scale subsidence suppresses convective activity, inhibiting the transport of water vapor into the free atmosphere. Although the ECMWF model is qualitatively successful in capturing the dry regions of the subtropics, the absolute magnitude of the local minima are too small, suggesting that it underpredicts the impact of large-scale atmospheric subsidence in lowering the TPW. The CCM, on the other hand, is more succesful in simulating this feature but tends to overpredict the value of TPW* over the summer hemisphere midlatitudes.

4.3. Temporal Variability

Figure 9 shows the standard deviation of daily TPW values calculated at each grid box for the SSM/I, ECMWF model, and CCM. For brevity the results have been zonally averaged. The main features in the observations are (1) a maximum in variability between 30^o and 60^o latitude, highlighting the impact of transient eddies associated with the mid latitude storm tracks, and (2) a minimum in variability over tropical to subtropical latitudes and over the very dry high-latitude oceans. Interestingly, a band of minimum variations, closely coinciding with the band of maximum monthly mean TPW (compare Figure 3), is clearly evident along the ITCZ. This feature is somewhat surprising in that one might expect to see the largest variations in these areas, since they have a larger potential range of values to occupy. This low variability may reflect a

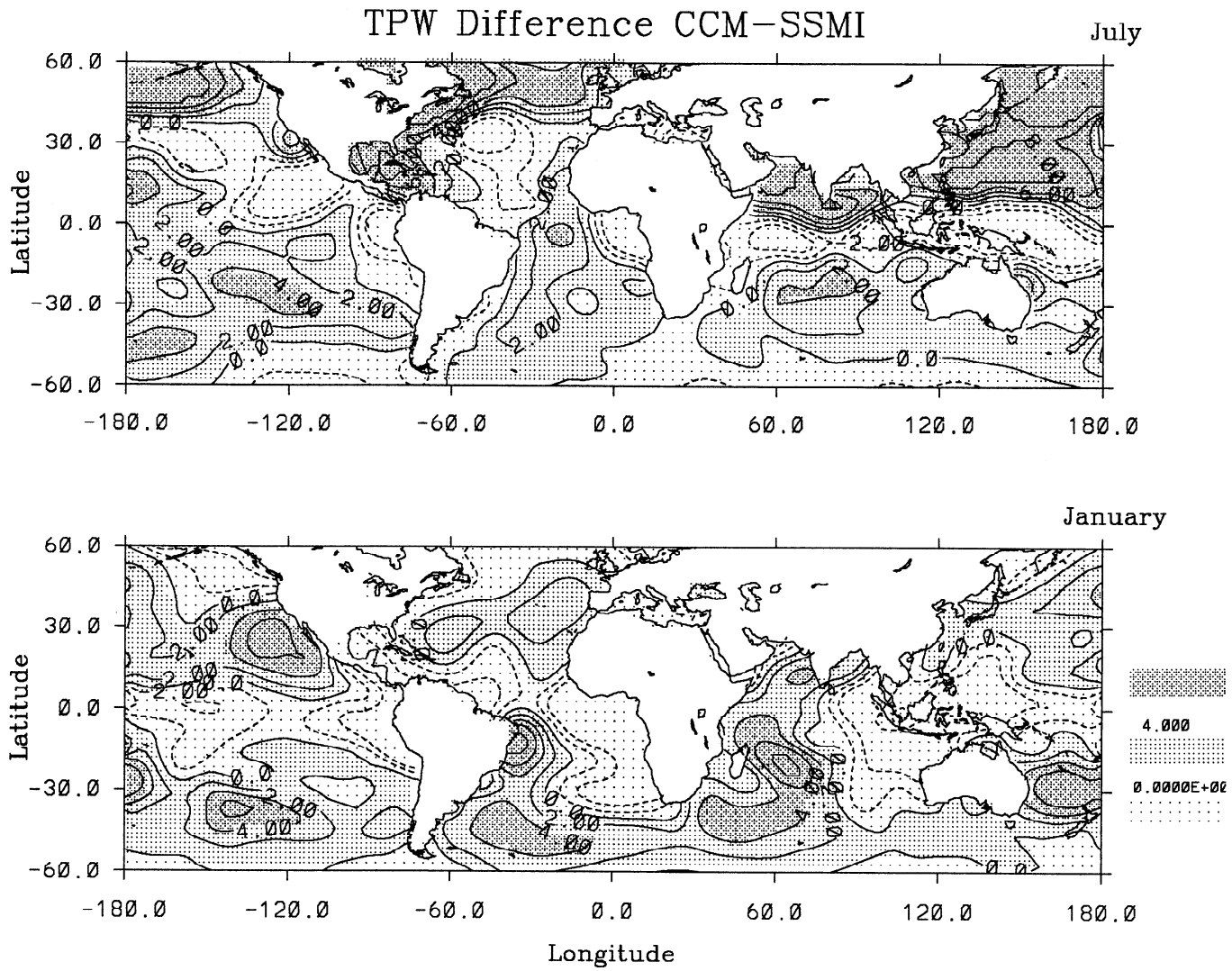

Fig. 7. Difference in TPW (CCM - SSM/I) for (top) July 1987 and (bottom) January 1988.

lack of sensitivity in the NESDIS retrieval algorithm under very moist conditions due to saturation of the 22-GHz channel despite improvements in the algorithm intended to correct this problem [see Alishouse et al., 1990]. However, the standard deviations in the ECMWF analyses also exhibit a similar band of low variability along the ITCZ, suggesting that this feature is in fact real. Given the strong dependence of TPW on SST, a possible explanation of the low variability may be the smooth nature of tropical SSTs. However, the CCM uses observed SSTs but simulates a local maximum in the variability along the ITCZ, indicating that dynamical processes are also important in determining the variability.

The daily standard deviation in TPW for the ECMWF model is very similar to that calculated from the SSM/I observations, highlighting the success of the ECMWF model in capturing the transient activity of TPW on shorter time scales. However, inspection of the CCM simulations reveals a pattern of excessive variability over tropical and midlatitude convective regions. The fact that the excessive variability in TPW tends to coincide with known areas of convective activity suggests a problem in parameterizing the transport of water vapor by deep convection. Figure 10 compares a time series plot of TPW from the SSM/I, ECMWF model, and CCM for a single grid box (140° W, 10° N) for 31 days from July 9 to August 8, 1987. The CCM values tend to exhibit a much larger range of variability than the observed values, with a quasi-periodic oscillation between exceedingly low and exceedingly high values of TPW. The excessive range of TPW is at least partially responsible for the greater variability and suggests that the model is allowing the atmosphere to reach an unrealistically dry and quiescent state and then compensating for this by producing an excessive moistening of the atmosphere when convection does occur. The excessive variability may also reflect the absence of a prognostic cloud variable in the CCM. When condensation occurs in the model, all condensed water is assumed to precipitate out, whereas in reality some condensate remains and eventually reevaporates, acting to dampen the variability in TPW.

5. Upper Tropospheric Water Vapor

Since the saturation vapor pressure of water decreases exponentially with temperature according to the Clausius-

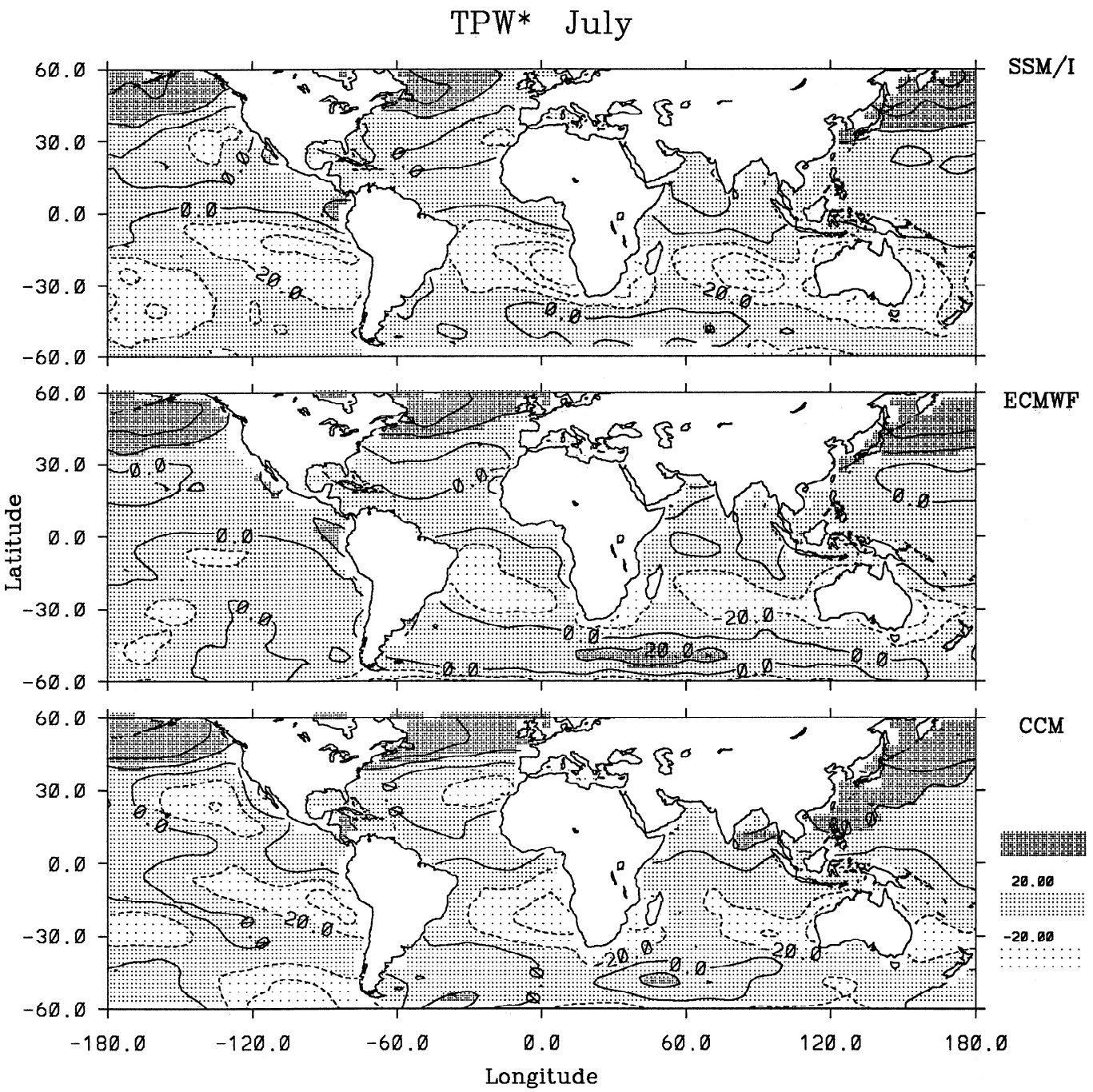

Fig. 8. Same as Figure 3 but for TPW*. Numbers are percentages.

Clapeyron relationship, and since temperature decreases with height, the vertically integrated mass of water vapor largely reflects the amount of water vapor in the lower troposphere. However, because of its cold radiating temperature, upper tropospheric water vapor is of significant importance in determining the amount of IR radiation trapped by the atmosphere. Accurate simulations of upper tropospheric water vapor are also necessary if GCMs are to be able to predict the formation and dissipation of cirrus clouds, which strongly modify the IR radiation emitted to space. To evaluate the ability of the ECMWF model and CCM to the simulate the distribution of upper tropospheric water vapor, we compare the monthly mean and temporal variability of the $T_{6.7}$ calculated using the models' profiles of temperature and moisture with the observed clear-sky $T_{6.7}$ from GOES 7.

As with the TPW, it is necessary to evaluate the significance of the differences between the CCM and the observations by examining the magnitude and distribution of interannual variability. The standard deviations of monthly mean $T_{6.7}$ (Figure 11) calculated from 20 January and July time periods of CCM simulations are once again used as a surrogate measure of interannual variability. Maximum variability in the CCM $T_{6.7}$ ranges from 2 to 3 K and tends to coincide with regions of large-scale subsidence over the subtropics, while convective areas of

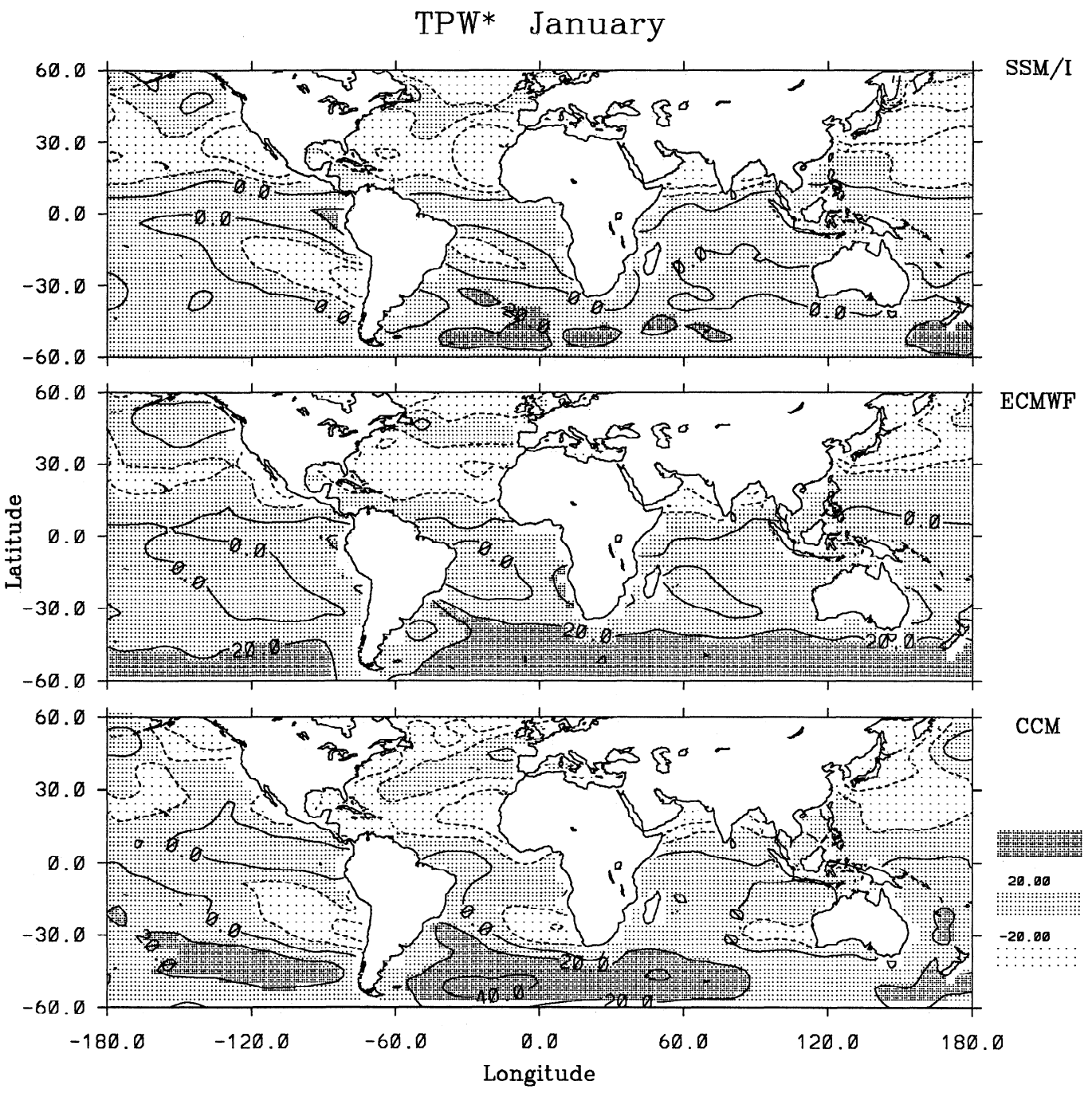

Fig. 8. (continued)

the tropics and midlatitudes are generally characterized by smaller interannual variations.

5.1. *Monthly Mean* $T_{6.7}$

Figures 12*a* and 12*b* show the distribution of the observed monthly mean clear-sky $T_{6.7}$ corresponding to the GOES viewing domain for July 1987 and January 1988. The $T_{6.7}$ is primarily sensitive to relative humidity vertically averaged over a range of pressures in the upper troposphere extending from roughly 200 to 500 mbar (see Figure 1). Warm temperatures indicate a dry upper troposphere, whereas cold temperatures correspond to a wet upper troposphere. A systematic decrease in $T_{6.7}$ toward the edge of the observational domain results from an increase in atmospheric path due to the increase in satellite-viewing zenith angle away from the subsatellite point. As a result, a greater portion of the upwelling radiation at the top of the atmosphere is received from higher, colder levels, resulting in lower $T_{6.7}$. This effect is commonly known as "limb darkening". Further inspection of Figure 12 reveals a distinct zonal pattern in both months, highlighting the impact of the large-scale circulation upon the distribution of upper tropospheric water vapor. In July, the warmest $T_{6.7}$ (240-255 K) occurs in a band over the southern hemisphere subtropics stretching from

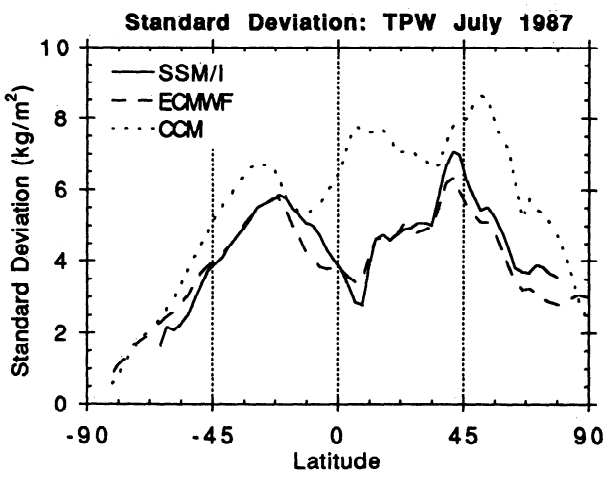

Fig. 9. Zonally averaged standard deviation of TPW for SSM/I observations, ECMWF analyses, and CCM simulations for (top) July 1987 and (bottom) Janaury 1988. Units are kilograms per square meter.

the eastern Pacific ocean across South America. In the northern hemisphere subtropics, maximum $T_{6.7}$ occurs off the west coast of Baja California with lower $T_{6.7}$ stretching across the central United States and into the subtropical Atlantic Ocean. A similar pattern is evident for January; however, the maximum $T_{6.7}$ values have now shifted south by roughly 5°-10° latitude, and the two branches now join over the eastern Pacific rather than the western Atlantic. These bands of maximum $T_{6.7}$ correspond to the regions of large-scale atmospheric subsidence associated with the descending branches of the Hadley circulation. The noticeable asymmetry in the warm $T_{6.7}$ between the northern and southern hemisphere in both seasons reflects the increased strength of the Hadley cell-driven subsidence over the winter hemisphere. Minimum $T_{6.7}$ values tend to occur in a narrow band separating the northern and southern hemisphere subtropical maxima. These minima result from deep convection along the ITCZ which moistens the upper troposphere and reduces the outgoing 6.7-μm radiation. Colder $T_{6.7}$ is also present over the convectively

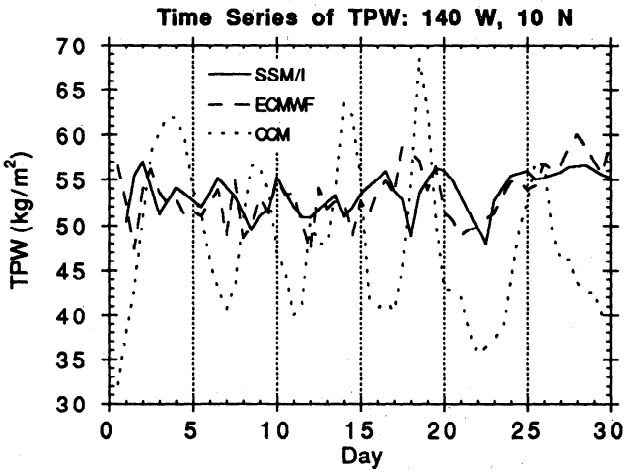

Fig. 10. Time series of TPW for July 9 to August 8, 1987, from SSM/I observations, ECMWF analyses, and CCM simulations.

active regions of the northern and southern hemisphere midlatitudes. At these latitudes, baroclinic instability drives convection associated with synoptic scale storms, which moistens the upper troposphere and lowers the outgoing $T_{6.7}$.

The monthly mean forward calculated $T_{6.7}$ values based on ECMWF analyses, CCM simulations are also shown for both months in Figures 12*a* and 12*b*. The ECMWF model is successful in predicting the basic features present in the observed distribution. In particular, the ECMWF model accurately captures the tropical minima, the subtropical maxima, the asymmetry between the northern and southern hemisphere maxima, and the seasonal variation of this assymetry. There are, however, noticeable discrepancies between the analyses and the observations. The most obvious is the underprediction of the gradient between the ascending regions of the tropics where the ECMWF is too warm (dry) and the descending regions of the subtropics where the ECMWF is too cold (moist). This discrepancy is consistent with the findings of *Eyre* [1992] who noted a similar pattern in the bias corrections for TOVS. Figure 13 shows the difference in $T_{6.7}$ (ECMWF - GOES) for both

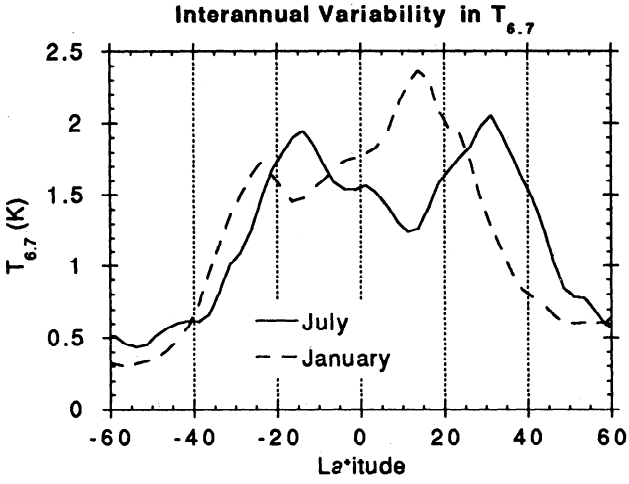

Fig. 11. The interannual standard deviation of monthly mean $T_{6.7}$ determined from a 20-year CCM simulation. Units are Kelvin.

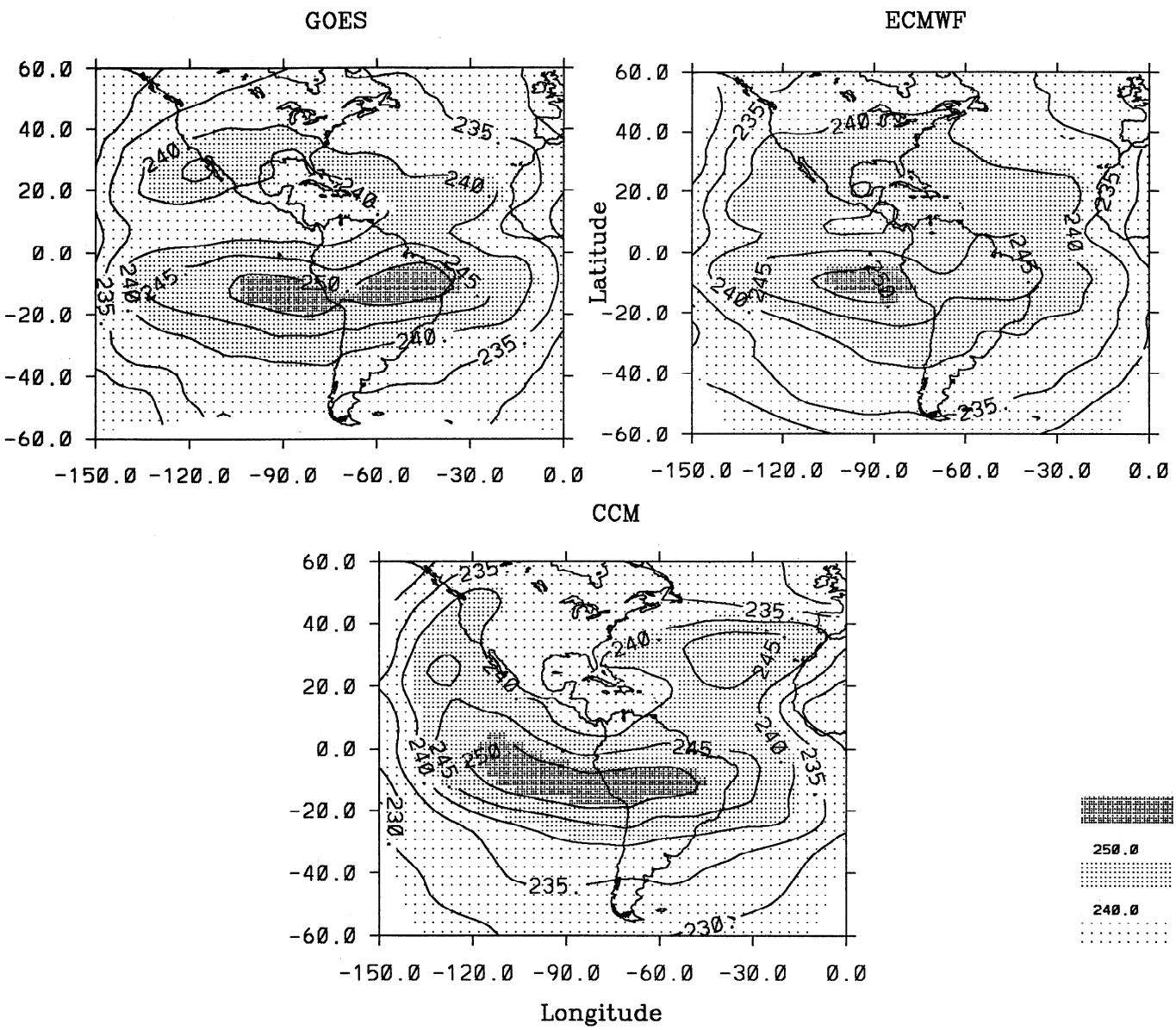

Fig. 12. Monthly mean $T_{6.7}$ from GOES observations, ECMWF analyses, and CCM simulations for (a) July 1987 and (b) Janaury 1988. Units are Kelvin.

periods. Small positive differences are evident over parts of the southern and northern hemisphere midlatitude storm tracks in both seasons, suggesting a slight underprediction in the upward transport of water vapor over these regions. Slightly larger positive biases of 2 to 4 K are present in a band along the ITCZ in July and over convective regions of Brazil and the tropical Atlantic January. Similarly, large negative biases ranging from -2 to -4 K dominate most of the northern and southern hemisphere subtropical oceans in both seasons.

It is worth recalling that the observed $T_{6.7}$ values are subject to a potential clear-sky (dry) sampling bias (compare Table 1). However, over regions of deep convection (e.g., ITCZ) where this effect is likely to be largest the observations are moister than the model. In comparison, the observations are dryer than the model over the subtropics, where upper level cloud cover is rare and clear-sky sampling biases are not important. Hence, sampling biases resulting cloud clearance do not explain the observed pattern of discrepancy. It is possible that the lower observed $T_{6.7}$ over the tropics is a result of cloud contamination; however, cloud contamination can not explain the warmer observed $T_{6.7}$ over the subtropics. Rather, the reduced moisture contrast between the tropics and subtropics may be due to an underprediction in the strength of the Hadley circulation. For example, studies

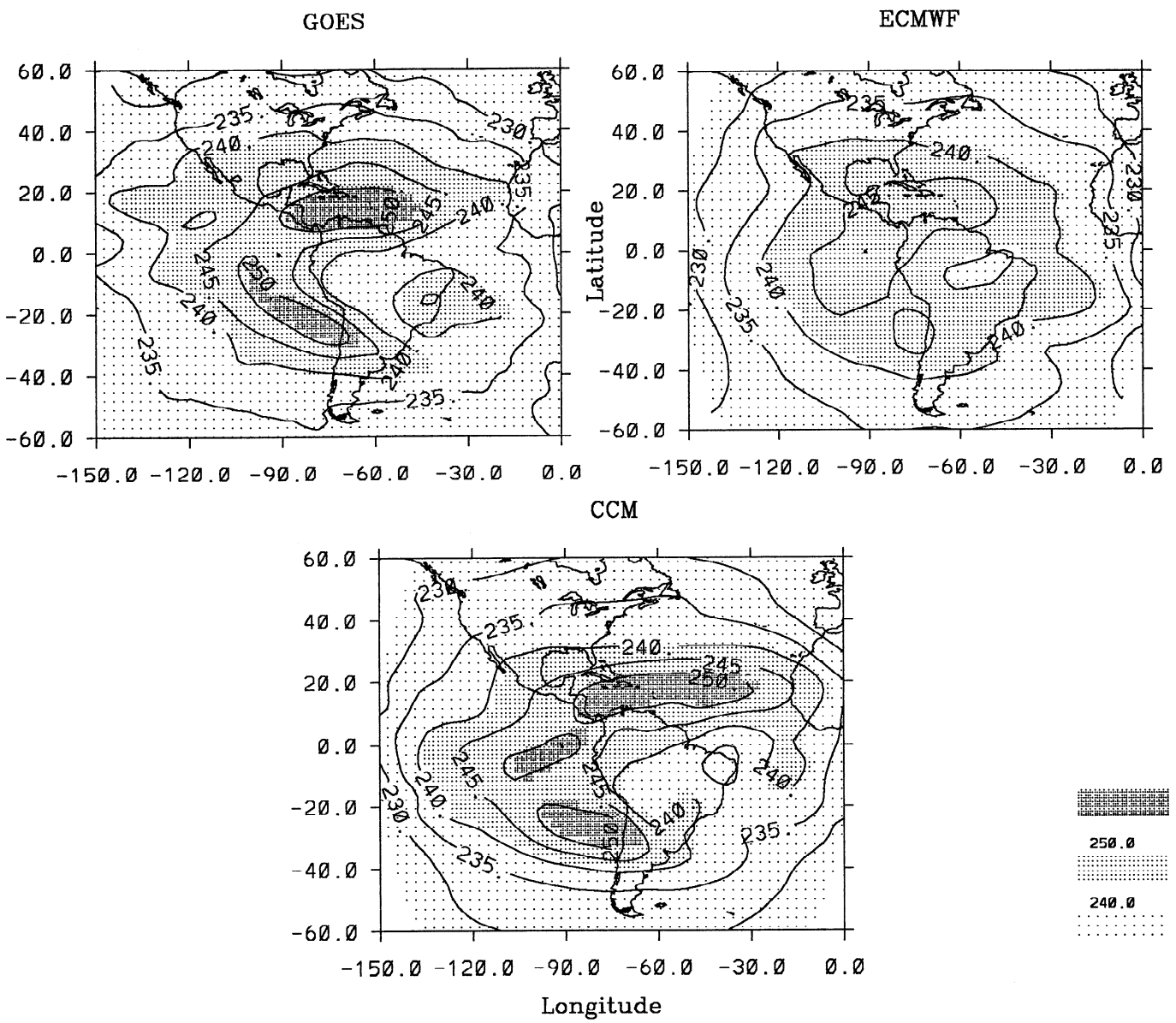

Fig. 12. (continued)

with the CCM version 1, [*Kichl and Williamson*, 1991] have shown that a stronger Hadley circulation dries the upper troposphere in regions of subsidence (e.g., in the subtropics) and moistens the upper troposphere in regions of convection (e.g., in the ITCZ). An interesting possibility is that the observed pattern of moisture bias could contribute to the weakened Hadley circulation by decreasing the amount of IR radiation absorbed in the tropics and increasing it in the subtropics. Since the large-scale circulation in turn influences the upper tropospheric water vapor distribution, this relationship demonstrates a possible feedback between upper tropospheric water vapor, IR radiation, and large-scale circulation. Finally, we note that in May 1989 the convective parameterization in the ECMWF model was changed from a Kuo scheme to a mass flux scheme. Although the change in convective parameterizations could significantly affect the distribution of moisture in the upper troposphere, a comparison between TOVS measurements of $T_{6.7}$ and ECMWF analyses for 1991-1992 indicates a similar pattern of discrepancy [*Eyre*, 1992].

The $T_{6.7}$ values calculated from the CCM simulations also capture the basic features of the observed distribution, including the positions, magnitudes and seasonal variations of the subtropical maxima. However, the CCM simulations exhibit less spatial agreement with the observations than the ECMWF analyses do. This is most evident in July, when a clearly defined band of cold (wet) $T_{6.7}$ associated with the ITCZ is missing. In the northern hemisphere, the CCM is considerably warmer (dryer) than observations over the subtropical Atlantic and Pacific Oceans, while it is

TABLE 1. Bias Estimates in Clear-Sky $T_{6.7}$.

	60° S - 30° S	30° S - 0	0 - 30° N	30° N - 60° N
Bias, K	-0.52	-0.05	-0.13	-0.12

Values represent the difference between the monthly mean ECMWF $T_{6.7}$ and the mean ECMWF $T_{6.7}$ averaged from only those grid boxes in which a corresponding clear-sky $T_{6.7}$ was available from GOES.

colder (wetter) over the central United States. In January, the CCM simulations are better than the ECMWF analyses in capturing the warm (dry) subtropical $T_{6.7}$, although the minimum over the northeast corner of Brazil is not present in the observations. In comparison to the ECMWF results, the CCM $T_{6.7}$ differences (Figure 14) do not correspond as closely to well-known features of the large-scale circulation. The differences in $T_{6.7}$ (which frequently exceed 4 K) are typically a factor of 2 larger than interannual variations estimated from the CCM, suggesting that they represent a real bias in the model. One reason for the poorer spatial agreement in $T_{6.7}$ for the CCM relative to the ECMWF model is partially due to the assimilation of TOVS retrievals into the ECMWF analysis. Another reason may be the spatial resolution at which the model integrations were performed. The CCM was run at a T42 spatial resolution ($\approx 2.8^o$ latitude/longitude), while the ECMWF forecasts were performed at a T106 resolution ($\approx 1.1^o$ latitude/longitude). This is consistent with the

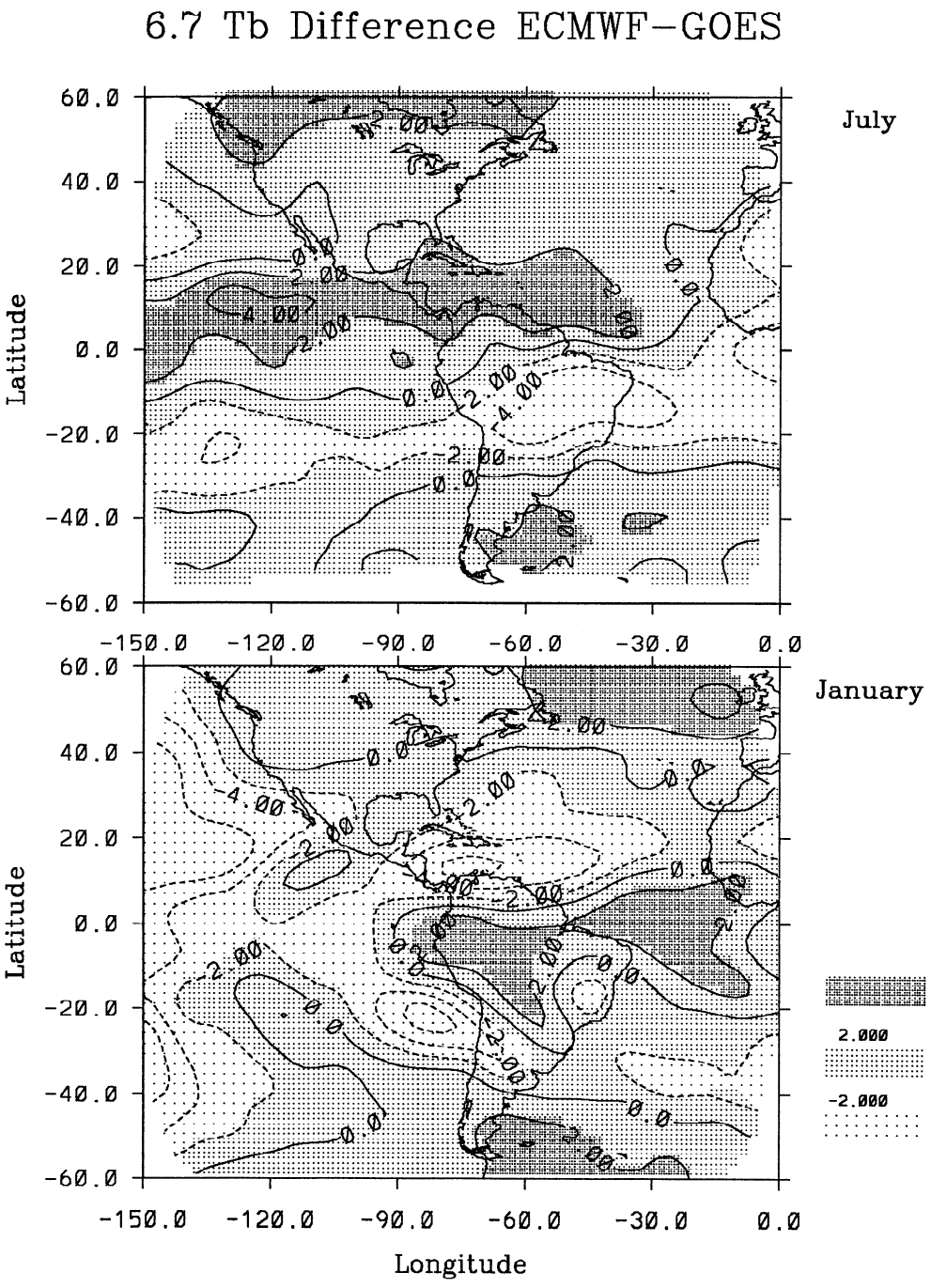

Fig. 13. Difference in $T_{6.7}$ ECMWF - GOES for (top) July 1987 and (bottom) January 1988.

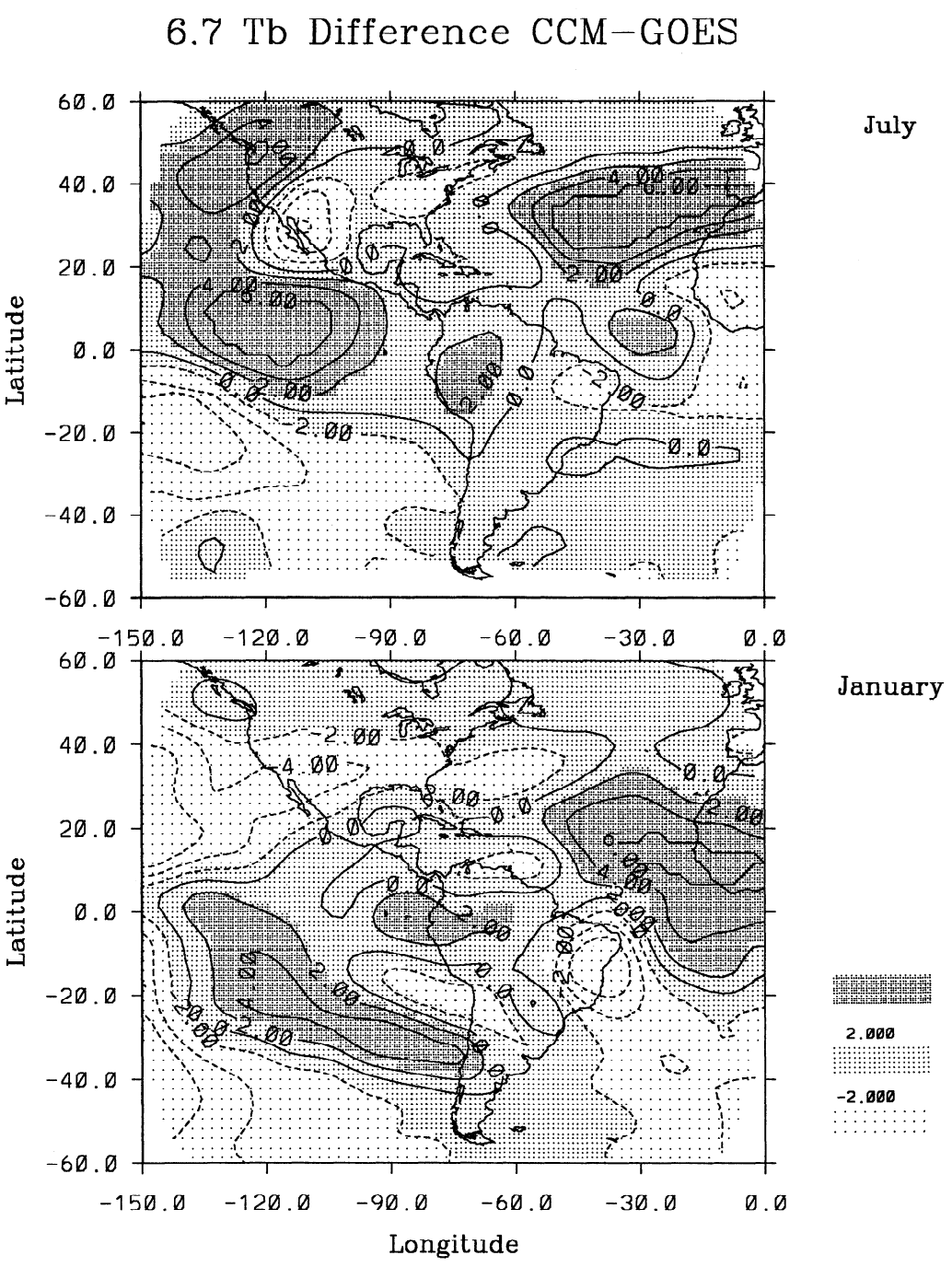

Fig. 14. Same as Fig. 13 but for CCM- GOES.

study by *Kiehl and Williamson* [1991] which demonstrated that increasing the model resolution results in a more realistic depiction of the physical process associated with deep convection.

5.2. Upper Tropospheric Humidity (UTH) Interpretation

Although comparing the observed and simulated $T_{6.7}$ is an appropriate means of evaluating a model's ability to simulate the distribution of upper tropospheric water vapor, for interpretation purposes it is useful to relate the observed and simulated brightness temperatures to a more physically meaningful quantity. For this purpose, *Soden and Bretherton* [1993] developed an interpretation tool based upon a simplified treatment of the radiative transfer at 6.7 μm. They demonstrated that, accurate to about $\pm$ 1 K, the $T_{6.7}$ can be related to the relative humidity vertically averaged over a range of pressures in the upper troposphere according to

$$\log\left(\frac{\mathrm{UTH}}{cos\theta}\right) = a + bT_{6.7} \qquad (3)$$

where UTH is the vertically averaged upper tropospheric relative humidity, θ is the satellite zenith angle, and a = 31.50 and b = -0.115 K^{-1} are regression coefficients.

For consistency, the distributions of UTH for the GOES, ECMWF model and CCM are calculated for each day by inverting (3) and inserting the appropriate zenith angle and the corresponding observed or calculated value of $T_{6.7}$.

Figures 15*a* and 15*b* show the resulting monthly mean UTH estimates for July 1987 and January 1988. Many features which were previously obscured by the zenith angle dependence of $T_{6.7}$ now become more apparent. During July, maxima in the observed UTH are now more clearly evident and coincide with convectively active regions along the ITCZ, Central America, southern hemisphere midlatitudes, and much of the North Atlantic. Dry regions form a distinct band along the southern hemisphere subtropics and over the subtropical ridges off the west coast of North America and northwest Africa. During January, the peak UTH which was over Central America has shifted south to Brazil and the UTH associated with the northern hemisphere storm tracks is now larger than the southern hemisphere values, reflecting the increase in baroclinic convection during winter. It is interesting to note that the seasonal variations of UTH over the midlatitudes, that is moister during winter and dryer during summer, are the opposite of those observed (and modeled) for TPW*. This suggests that UTH is more strongly influenced by the seasonal enhancement baroclinic convection during winter, whereas the changes in TPW* are determined by the seasonal variations in low-level moisture advection (compare section 4.2). It is also noted that the sign of the seasonal variation in UTH for the observations and both of the models agree; however, it tends to oppose that noted by *Rind et al.* [1991] in a study of water vapor feedback using Stratospheric Aerosol and Gas Experiment II (SAGE

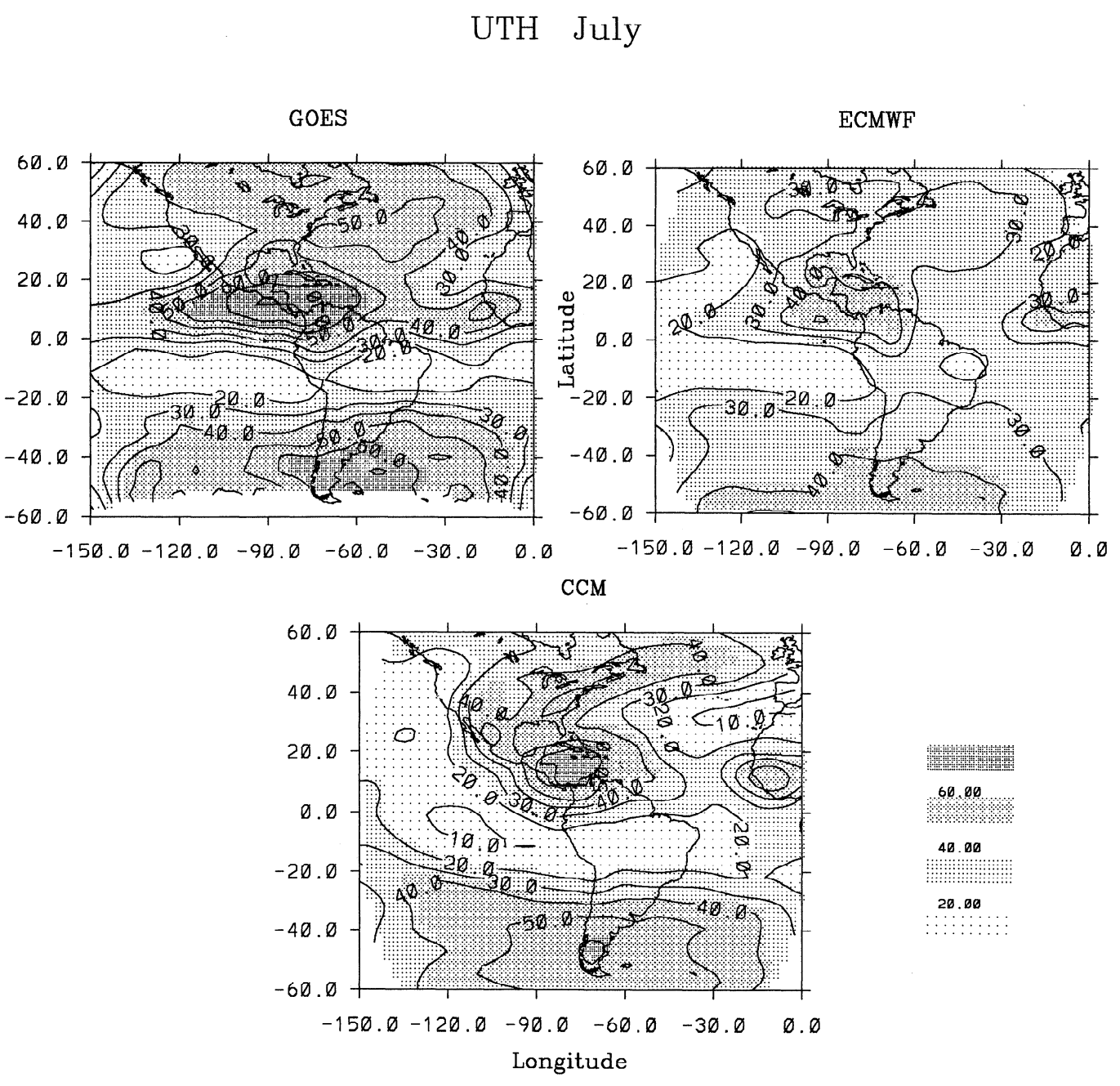

Fig. 15. Same as Figure 13 but for UTH. Numbers are percentages.

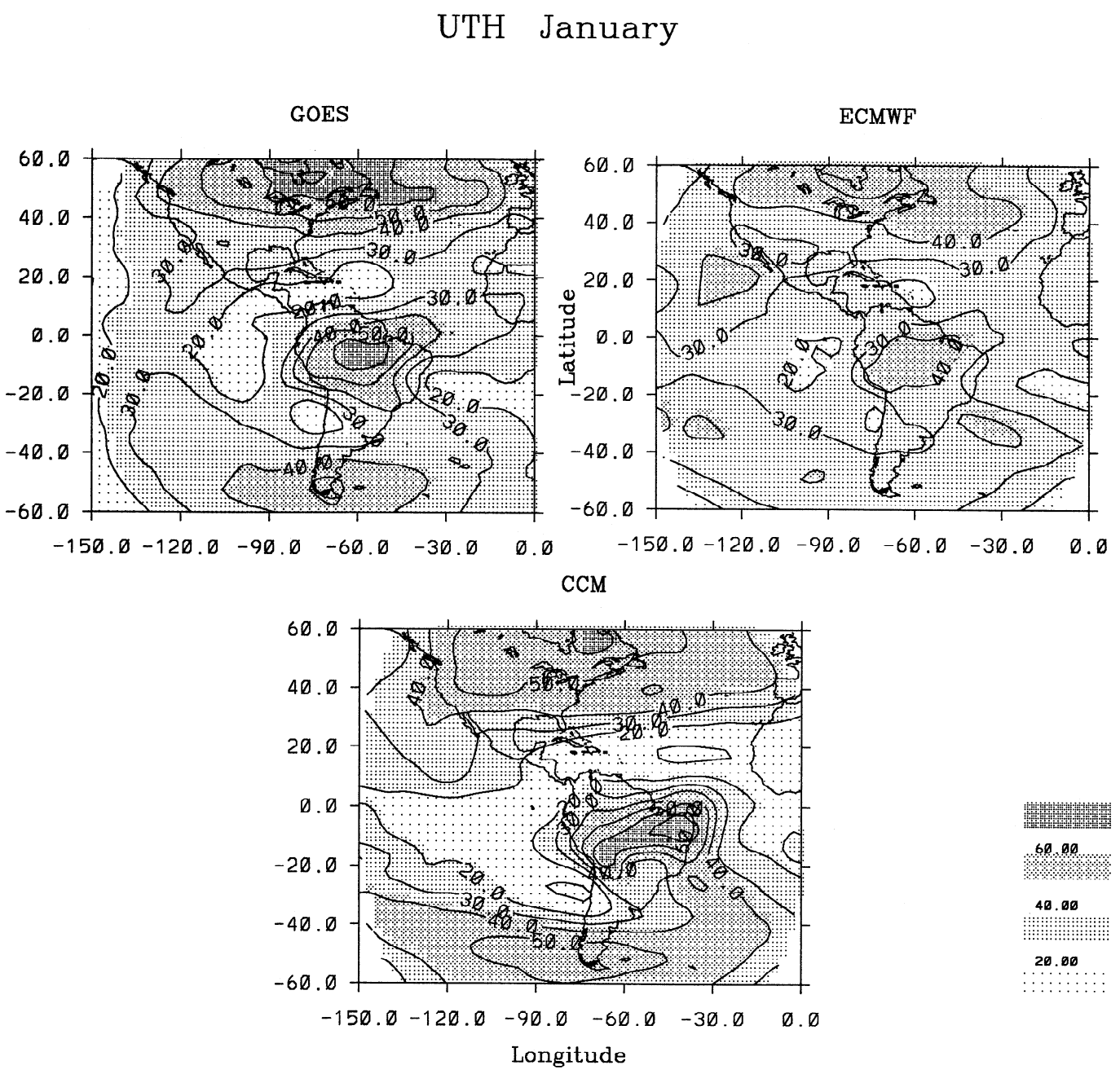

Fig. 15. (continued)

II) observations and Goddard Institute for Space Studies (GISS) GCM simulations. This may be attributable to differences in the vertical sensitivity of the measurements, differences in longitudinal sampling, or to simplifications used in deriving (3). However, further research is required to fully understand the differences.

The ECMWF model is successful in capturing the basic patterns of the observed UTH distribution and its seasonal variation; however, many of the discrepancies noted previously now become more obvious. During July, the underestimation of UTH along the ITCZ and the storm track area of the North Atlantic is more clearly demonstrated, as is the tendency for the ECMWF model to overestimate the moisture over regions of subtropical subsidence. In January, the ECMWF model correctly captures the maximum over the convective regions of Brazil; however, it overpredicts the UTH associated with subtropical dry bands. These patterns of discrepancy further illustrate the dry bias in convective regions and the moist bias in subsidence regions and are consistent with the earlier conclusion that the differences stem from a weakened Hadley circulation.

The CCM also captures the main features of UTH and their seasonal variation. However, it is somewhat less successful in reproducing details of the magnitude and distribution of these features. The most significant differences are the tendency to overestimate the peak values of UTH associated with tropical convection and the

midlatitude storm tracks. Other differences include the lack of a well defined ITCZ, particularly over the eastern Pacific in July, and a tendency to overestimate the dryness of the subtropics. These patterns of bias suggest a general tendency for the CCM to overestimate the UTH in regions of deep convection, both tropical and midlatitude.

From (3) it can be seen that the difference in the $T_{6.7}$ may be related to the difference in relative humidity according to,

$$bT_{6.7} = \Delta \log(\mathrm{UTH}) = \frac{\Delta \mathrm{UTH}}{\mathrm{UTH}} \quad (4)$$

Therefore, the proportional difference in vertically averaged humidity (i.e., relative or specific humidity) can be estimated by scaling the difference in $T_{6.7}$ by a factor of b = -0.115 K^{-1}. This provides a convenient tool for translating the differences in brightness temperature to a more interpretable quantity. Scaling the ECMWF - GOES differences (Figure 13) by this factor reveals proportional errors in the ECMWF upper tropospheric humidity of roughly 23% to 45% ($\Delta T_{6.7}$ = -2 to -4 K) in the regions of subtropical large-scale subsidence (e.g., descending branch of Hadley cell), 0% to 23% ($\Delta T_{6.7}$ = 0 to -2 K) over the northern and southern hemisphere midlatitudes, and -23% to -45% ($\Delta T_{6.7}$ = 2 to 4 K) over areas of deep tropical convection (e.g., ITCZ). For CCM - GOES (Figure 14), the differences tend to be larger, but systematic patterns of discrepancy are less obvious. In general, negative errors of -23% to -70% ($\Delta T_{6.7}$ = 2 to 6 K) tend to coincide with regions of apparent large-scale subsidence in the model, while positive differences of 23% to 45% ($\Delta T_{6.7}$ = -2 to -4 K) tend to be associated with regions of deep convection.

5.3. Temporal Variability

Figure 16 shows the standard deviation of daily samples of UTH estimated from the GOES, ECMWF model and CCM $T_{6.7}$. For brevity, only results from July 1987 are shown, since results for January lead to similar conclusions. Maximum variability in the observed UTH occurs primarily over two broad regions. One extends northward from the ITCZ over the eastern United States and western North Atlantic, while the other occupies most of the southern hemisphere midlatitudes. Minimum variations coincide with the dry regions of southern hemisphere subtropics and off the west coast of Baja California. The ECMWF model captures most aspects of this distribution but tends to underpredict the variability in UTH along the ITCZ and northeast coast of the United States. The reduced variability of UTH in the tropics may reflect a problem in correctly simulating the frequency and strength of water vapor transport into the upper troposphere by deep convection. In contrast to the ECMWF model, the CCM significantly overpredicts the variability in UTH over a large region covering Central America and the southern United States. These regions also exhibited excessive variability in TPW, suggesting a systematic overestimate of the temporal fluctuations of moisture at all levels.

6. Evaluation of Synoptic Variations in the ECMWF Model Water Vapor Fields

In addition to examining the distribution of water vapor on monthly mean time scales, it is also insightful to compare the observed and modeled water vapor fields on shorter, synoptic time scales. This is particularly relevant for the ECMWF model, since one of its primary functions is medium-range (3 to 6 day) weather prediction. This section examines the ability of the ECMWF analyses to properly simulate the synoptic sequence of the water vapor distribution as determined by the SSM/I and GOES observations. Since the CCM simulations are forced only with the observed sea surface temperatures, the simulated water vapor fields are not intended to capture the observed daily progression and are therefore not described in this section. To compare the observed and predicted TPW fields, the SSM/I observations are linearly interpolated onto 0000 and 1200 UT grid from the nearest available ascending (0612 equatorial passing time) and descending (1812 equatorial passing time) orbits. For the UTH, both the GOES and ECMWF data are available at 0000 and 1200 UT and no temporal interpolation is necessary.

6.1. Coherence of the Water Vapor Fields

One measure of the model's ability to track the day-to-day progression of the water vapor field can be obtained by examining the fraction of the observed variance explained by the model. Before beginning the comparison, it is beneficial to remove high-frequency noise in the water vapor fields. For the observations, this variability may stem from errors associated with the 6.7-μm cloud clearance, TPW retrieval, temporal interpolation, or sensor noise. For the ECMWF analyses high-frequency noise may be associated with model spin-up or spurious gravity waves induced by data assimilation. Although uninitialized analyses were selected for this study because of their accessibility, future comparisons may be improved by using initialized analyses or short-term forecasts to help minimize high-frequency noise. To isolate this high-frequency variability from the more meaningful synoptic-scale fluctuations, the observed and modeled time series for each grid box are expanded into sine and cosine components and filtered in the time domain. A band-pass filter which emphasizes fluctuations with periods (P) between roughly 3 and 30 days is used, and the squared correlation of the observed and modeled water vapor fields, commonly referred to as the coherence, is calculated. This procedure enables the comparison to ignore variance associated with high-frequency noise and focus on the more relevant synoptic-scale fluctuations.

Figure 17 depicts the zonally averaged coherence between the band-pass-filtered water vapor fields for (top) TPW and (bottom) UTH. For TPW, the coherence of band- pass fluctuations is greatest over the midlatitudes, where the fraction of explained variance ranges from 0.5 to 0.7. In contrast, the coherence is noticeably lower over the tropics, where the explained variance typically ranges from 0.3 to 0.4. This indicates that the model is more successful in tracking the water vapor fluctuations associated with midlatitude transient eddies than those associated with tropical disturbances. A partial explanation for the low coherence over the tropics may be the low temporal variability in TPW observed for this region (compare Figure 9), which results in a smaller signal for the model to capture. For UTH, the fraction of explained variance in the model is markedly lower than it is for TPW, with typical values ranging from 0.1 to 0.4. However, a latitudinal dependence similar to that of TPW is noted,

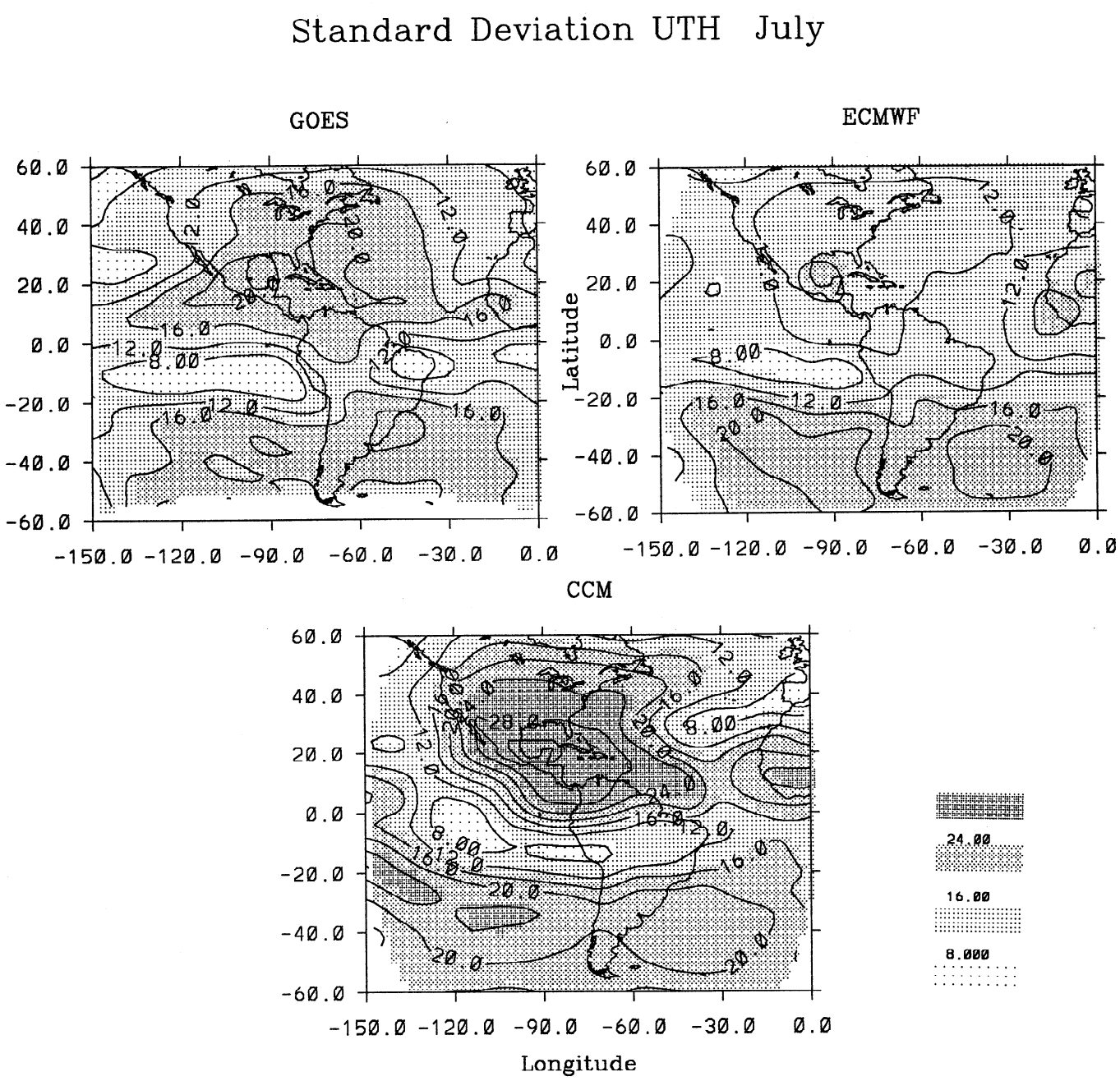

Fig. 16. Standard deviation of UTH for GOES observations, ECMWF analyses, and CCM simulations for July 1987. Numbers are percentages.

with maximum coherence over the midlatitudes and minima along the tropics. The lower coherence noted for the tropics is consistent with the earlier hypothesis that the simulation of water vapor transport via the Hadley cell is deficient. This pattern also suggests that the ECMWF model is more successful in tracking fluctuations in UTH associated with midlatitude baroclinic disturbances than those associated with tropical convection. This may reflect a greater difficulty in parameterizing tropical deep convection, which is characterized by subgrid vertical instabilities, whereas midlatitude convection is associated with much larger scale baroclinic processes. This conclusion is consistent with recent studies [e.g., *Kasahara et al.*, 1993] which suggest that vertical velocities predicted by global analysis models in the tropics are unreliable owing to the lack of accurate diabatic initialization and the failure of simple mass-wind relationships at low latitudes.

For reference, the high-pass (1 to 3-day) coherence of both TPW and UTH is also plotted in Figure 17. Over most latitudes, the coherence in the high-pass frequency components is typically a factor of 4-10 lower than that for the band-pass components. An extreme interpretation of this is that there is little skill in the short-term (< 3-day) model forecasts and that the increased agreement on longer time scales is primarily attributable to the assimilation of TOVS water vapor fields. An alternative interpretation is that the high-frequency fluctuations are dominated by noise in the data and that the model demonstrates real

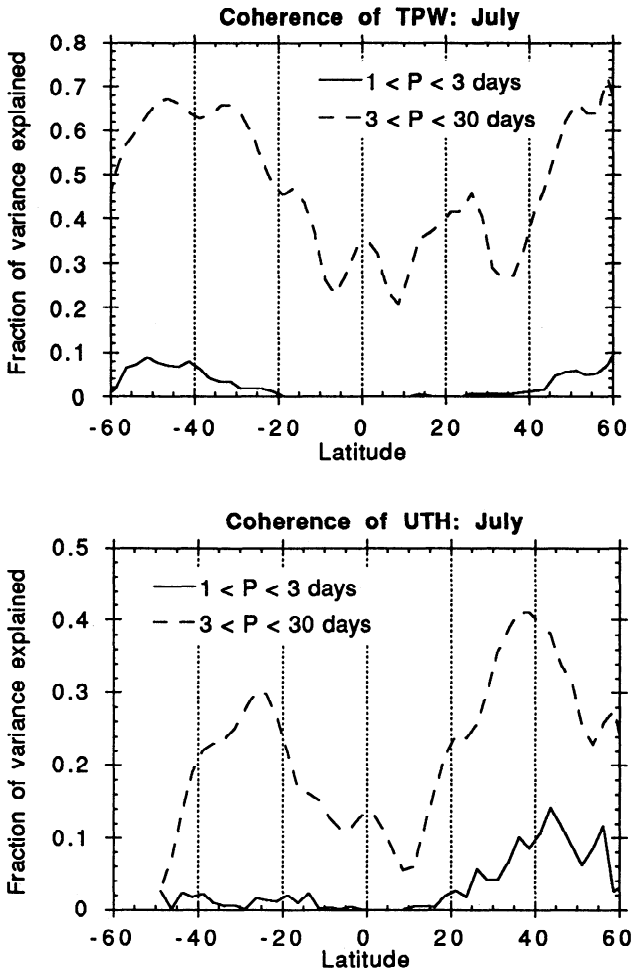

Fig. 17. The zonally averaged band-pass (3 to 30-day) filtered coherence for (top) TPW and (bottom) UTH. Results are for July 1987.

forecasting skill, as evidenced by the greater agreement for longer synoptic-scale fluctuations. Our inclination is toward the latter interpretation; however, further analysis is needed to fully establish this.

6.2. *Percentage of Values Within Observational Uncertainty*

A slightly different perspective of the success of the ECMWF model in capturing the synoptic-scale fluctuations of the water vapor field is obtained by examining the number of model forecasts for which the predicted TPW or UTH is within the estimated observational uncertainty for that quantity. To remove the apparent high-frequency noise in the data sets, both the modeled and observed water vapor fields are smoothed using a 3-day running average filter. Since the absolute values of TPW and UTH can vary by nearly an order of magnitude, greatest insight is obtained by comparing the relative difference (rather than the absolute difference) between the satellite observations and ECMWF analyses, that is (satellite - ECMWF)/satellite. Using the data of *Alishouse et al.* [1990] (see their Table 3), the relative uncertainty the TPW retrievals is estimated to be $\epsilon_{\mathrm{TPW}} \approx 0.12$. For the observational error in UTH, *Soden and Bretherton* [1993] demonstrated the observed clear-sky $T_{6.7}$ to be repeatable between successive 30 minute images to roughly 0.5-1.5 K. Using 1.5 K as a conservative estimate of the random error in the clear-sky 6.7-μm brightness temperature $\Delta T_{6.7}$, the relative uncertainty in the UTH observations (ϵ_{UTH}) can be calculated according to (4) as

$$\epsilon_{\mathrm{UTH}} = \frac{\Delta UTH}{UTH} = b\Delta T_{6.7} \approx 0.17 \qquad (5)$$

Since the observational uncertainties ϵ_{TPW} and ϵ_{UTH} represent only rough estimates, they are not intended to indicate the precise number of correct TPW or UTH predictions in the model. Rather, they are derived simply to provide a benchmark against which the differences between the model and the observations can be compared.

Figure 18 illustrates the percentage of values within $\pm\epsilon$ for both TPW and UTH. For brevity the results have been zonally averaged. As with the monthly mean quantities, the UTH again appears to be the most difficult of the two water vapor fields to capture, with only 10-40% of the predictions occurring within the estimated observational uncertainty. In comparison, almost all TPW percentages are greater than 40%. The TPW curves exhibit a strong latitudinal dependence with peak values over the tropics and decreasing values toward the poles. This is largely a reflection of the success of the model in predicting the monthly mean TPW for these latitudes, since there is very little temporal variability in the tropical TPW values. Examination of daily images of TPW from both the SSM/I and ECMWF suggests that the lower percentages noted for the midlatitudes are partially due to a smoothing of large TPW gradients in the model associated with frontal boundaries. The destruction of the sharp frontal boundaries is believed to result from the assimilation of satellite and radiosonde moisture profiles [*Zhang et al.*, 1989] near the fronts. For UTH a clear distinction between the tropics and midlatitudes is evident, with better daily agreement over the midlatitude storm tracks than over regions of deep convection in the tropics. The minima over the southern hemisphere subtropics does not necessarily indicate a discrepancy in the model's daily progression of UTH but rather is a reflection of the overall moist bias noted in the monthly mean for these regions.

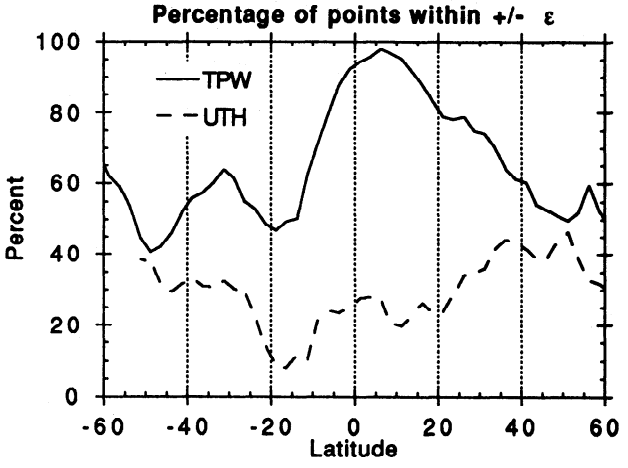

Fig. 18. The zonally averaged percentages of model analyses of TPW and UTH which are within the estimated observational uncertainty. Results are for July 1987.

7. SUMMARY

Overall, the results of the comparison are encouraging. Both the ECMWF model and the CCM are successful in simulating the primary features of the TPW and UTH distribution and their seasonal variation. This is clearly the requirement of greatest importance for GCMs. However, differences in details of the distribution are evident. For the ECMWF, discrepancies in TPW are primarily restricted to the subtropical ridges, where the predicted values are systematically 1.5 to 2 times larger than those observed. The CCM is more successful in capturing the subtropical minimum, but exhibits a distinct poleward shift in the peak TPW values over the northern hemisphere midlatitudes. Examination of the dynamical contributions toward the distribution of TPW demonstrates a reasonable degree of success on behalf of both models, although the ECMWF model exhibits a distinct moist bias over subsidence regions, while the CCM overestimates the convergence of moisture in midlatitudes. The temporal variability of TPW simulated by the ECMWF model agrees well the observations, exhibiting maximum standard deviations over the midlatitude storm tracks and minimum standard deviations along the ITCZ. The CCM, however, systematically overestimates the daily variations by up to a factor of 2 in tropical and midlatitude convective regions.

In comparison to the TPW, both the ECMWF model and the CCM tend to have greater difficulty simulating the spatial and temporal distributions of upper tropospheric relative humidity. This likely results from the greater dependence of UTH upon the large-scale circulation, while TPW is largely governed by the distribution of SST. The ECMWF is successful in capturing the basic features of UTH, however it clearly underpredicts the gradient in upper tropospheric water vapor between the ascending and descending branches of the Hadley cell, being too dry in the tropics and too wet in the subtropics. The distribution of UTH from the CCM simulations also illustrates the basic features present in the observations, yet it exhibits considerably less spatial agreement with the observations than the ECMWF analyses do. In contrast to the ECMWF model however, the discrepancies in the CCM do not reveal systematic patterns of error in correspondence with well-known features of the large-scale circulation. As with TPW, the temporal variability of the UTH in convective regions is also overpredicted in the CCM.

Although the overall comparison is favorable, there are significant discrepancies which do suggest a few areas where improvements could be made. For the ECMWF model, the overprediction of TPW associated with the subtropical ridges appears to result from difficulty in simulating the moisture profile within the boundary layer and possibly the assimilation of biased TOVS retrievals. The inclusion of an explicit boundary layer parameterization and the exclusion of TOVS water vapor retrievals for these regions may improve the results. The ECMWF model also underestimates the contrast in upper tropospheric moisture between the tropics and subtropics, suggesting an underprediction in the strength of the Hadley circulation. In the CCM, the tendency to overestimate the temporal variability of both TPW and UTH is most noticeable over known areas of convective cloud cover, suggesting that some of the discrepancies in the CCM may result from difficulties in modeling the transport of moisture by convection or the lack of a prognostic cloud variable. It is worth noting that previous versions of the CCM have also exhibited excessive variability in radiative fluxes which were largely attributed to the lack of a prognostic cloud variable [*Smith and Vonder Haar*, 1991; *Soden*, 1992]. Although it is not immediately clear how it would affect this comparison, the inclusion of a prognostic cloud variable would provide an interesting study of the sensitivity of the simulated water vapor distribution to the parameterization of other hydrologic processes.

Acknowledgments. We thank S. Ackerman, L. Donner, and J. Eyre for constructive comments and suggestions; H. Woolf for assistance with the CIMSS transmittance model; J. Kiehl for providing the CCM simulations; the NCAR Data Support Section for providing the ECMWF analyses; and the NASA/WETNET program for providing the SSM/I data. This study was performed while one of the authors (B.J.S.) was a Visiting Fellow at the Space Science and Engineering Center, University of Wisconsin. B.J.S. was supported by a NASA Global Change Fellowship. Computational resources were provided by CIMSS.

REFERENCES

Alishouse, J., C., S. A. Snyder, J. Vongasthorn, and R. R. Ferraro, Determination of oceanic total precipitable water from the SSM/I, *IEEE Trans. Geosci. Remote Sens., 28*, 811-816, 1990.

Brankovic, C., Zonal diagnostics of the ECMWF 1984-1985 operational analyses and forecasts, *Tech. Rep. 57*, 72 pp., Eur. Cent. for Medium-Range Weather Forecasts, Reading, England, 1986.

Cess, R. D. et al., Intercomparison and interpretation of climate feedback processes in 19 atmospheric general circulation models, *J. Geophys. Res., 95*, 16,601-16,615, 1990.

Chahine, M. T., The global energy water cycle experiment, *EOS Trans. AGU, 73*, 9-14, 1992.

Elliott, W. P., and D. J. Gaffen, On the utility of radiosonde humidity archives for climate studies, *Bull. Am. Meteorol. Soc., 72*, 1507-1520, 1991.

Eyre, J. R., A fast radiative transfer model for satellite sounding systems, *Tech. Memo. 187*, Eur. Cent. for Medium-Range Weather Forecasts, Reading, England, 1991.

Eyre, J. R., A bias correction scheme for simulated TOVS brightness temperatures, *Tech. Memo. 186*, Eur. Cent. for Medium-Range Weather Forecasts, Reading, England, 1992.

Gaffen, D. J., and T. P. Barnett, A comparison of observations and model simulations of tropospheric water vapor, *J. Geophys. Res., 97*, 2775-2780, 1992.

Grody, N. C., A. Gruber, and W. C. Shen, Atmospheric water vapor content over the tropical Pacific derived from Nimbus-6 scanning microwave spectrometer, *J. Appl. Meteorol., 19*, 986-996, 1980.

Hack, J. J., B. A. Boville, B. P. Briegleb, J. T. Kiehl, P. J. Rasch, and D. L. Williamson, Description of the NCAR Community Climate Model (CCM2), *Tech. Note NCAR/TN-382+STR*, Natl. Cent. for Atmos. Res., Boulder, Colo., 1993.

Hollinger, J. P., R. Lo, G. Poe, R. Savage, and J. Pierce, *SSM/I Users Guide*, 120 pp., Naval Research Laboratory, Washington D. C., 1987.

Holtslag, A. A. M., and B. A. Boville, Local versus nonlocal boundary layer diffusion in a global climate model, *J. Clim., 6*, 1825-1842, 1993.

Illari, L., The quality of satellite precipitable water content data and their impact on analyzed moisture fields, *Tellus, 41A*, 319-337, 1989.

Intergovernmental Panel on Climate Change, *Climate Change: The IPCC Scientific Assessment*, 365 pp., Cambridge University Press, New York, 1990.

Kasahara, A., A. P. Mizzi, and L. J. Donner, Diabatic initialization for improvement in the tropical analysis of divergence and moisture using satellite radiometric imagery data, *Tellus*, in press, 1993.

Kiehl, J. T., and B. P. Briegleb, Comparison of the observed and calculated clear-sky greenhouse effect: Implications for climate studies, *J. Geophys. Res.*, *97*, 10,037- 10,049, 1992.

Kiehl, J. T., and D. L. Williamson, Dependence of cloud amount on horozontal resolution in the NCAR Community Climate Model, *J. Geophys. Res.*, *96*, 10955-10980, 1991.

Lindzen, R. S., Some coolness concerning global warming, *Bull. Am. Meteorol. Soc.*, *71*, 288- 299, 1990.

Liu, T. W., W. Tang, and F. Wentz, Precipitable water and surface humidity over global oceans for the SSM/I and ECMWF, *J. Geophys. Res.*, *97*, 2251-2264, 1992.

Moller, F. Atmospheric water vapor measurements at 6-7 microns from a satellite, *Planet. Space Sci.*, *5*, 202-206, 1961.

Prabhakara, C., G. Dalu, R. C. Lo, and N. R. Nath, Remote sensing of seasonal distribution of precipitable water vapor over the oceans and the inference of boundary layer structure, *Mon. Weather Rev.*, *107*, 1388-1401, 1979.

Prabhakara, C., H. D. Chang, and A. T. C. Wang, Remote sensing of precipitable water over the oceans from Nimbus-7 microwave measurements, *J. Appl. Meteorol.*, *21*, 59-68, 1982.

Rasch, P. J., and D. L. Williamson, Computational aspects of moisture transport in global models of the atmosphere, *Q. J. R. Meteorol. Soc.*, *116*, 1071-1090, 1990.

Raval, A., and V. Ramanathan, Observational determination of the greenhouse effect, *Nature*, *342*, 758-762, 1989.

Rind, D., E. W. Chiou, W. Chu, J. Larsen, S. Oltmans, J. Lerner, M. P. McCormick, and L. McMaster, Positive water vapour feedback in climate models confirmed by satellite data, *Nature*, *349*, 500-503, 1991.

Schmetz, J., and O. M. Turpeinen, Estimation of the upper tropospheric relative humidity field from METEOSAT water vapor image data, *J. Appl. Meteorol.*, *27*, 889-899, 1988.

Smith, L. D., and T. H. Von der Haar, Cloud-radiation interactions in a general circulation model: Impact upon the planetary radiation balance, *J. Geophys. Res.*, *96*, 893-913, 1991.

Soden, B. J., Validation of cloud forcing simulated by the NCAR Community Climate Model using observations from the Earth Radiation Budget Experiment, *J. Geophys. Res.*, *97*, 18,137-18,159, 1992.

Soden, B. J., and F. P. Bretherton, Upper tropospheric relative humidity from the GOES 6.7-μm channel: Method and climatology for July 1987, *J. Geophys. Res.*, *98*, 16,669-16,688, 1993.

Staelin, D. H., K.F. Kunzi, R. L. Pettyjohn, R. K. Poon, R. W. Wilcox, and J. W. Waters, Remote sensing of atmospheric water vapor and liquid water with the Nimbus 5 microwave spectrometer, *J. Appl. Meteorol.*, *15*, 1204-1214, 1976.

Stephens, G. L., On the relationship between water vapor over the oceans and sea surface temperature, *J. Clim.*, *3*, 634-645, 1990.

Trenberth, K. E., and J. G. Olson, An evaluation and intercomparison of global analyses from the National Meteorological Center and the European Centre for Medium Range Weather Forecasts, *Bull. Am. Meteorol. Soc.*, *69*, 1047-1057, 1988.

Wu, X., J. J. Bates, and S. J. S. Khalsa, A climatology of the water vapor band brightness temperatures from NOAA operational satellites, *J. Clim.*, *6*, 1282-1300, 1992.

Zhang, Z., J. Pailleix, and G. Kelly, Evaluation of developments of the ECMWF humidity analysis, *Tech. Memo. 160*, 31 pp., Eur. Cent. for Medium-Range Weather Forecasts, Reading, England, 1989.

F. P. Bretherton, Space Science and Engineering Center, University of Wisconsin-Madison, 1225 West Dayton Street, Madison, WI 53706.

B. J. Soden, Atmospheric and Oceanic Sciences Program, Princeton University, P.O. Box 308, Princeton, NJ 08542.

(Received June 3, 1993; revised October 12, 1993; accepted October 14, 1993.)